A&A 446, 643–660 (2006)
DOI: 10.1051/0004-6361:20053029

Astronomy & Astrophysics

α Eridani: rotational distortion, stellar and circumstellar activity⋆

M. M. F. Vinicius[1], J. Zorec[2], N. V. Leister[1], and R. S. Levenhagen[1]

[1] Instituto de Astronomia, Geofísica e Ciências Atmosféricas da Universidade de São Paulo, CUASO, 05508-900 São Paulo SP, Brazil
e-mail: vinicius@astro.iag.usp.br
[2] Institut d'Astrophysique de Paris, UMR 7095 CNRS – Université Pierre & Marie Curie, 98bis Boulevard Arago, 75014 Paris, France

Received 9 March 2005 / Accepted 14 September 2005

ABSTRACT

We explore the geometrical distortion and the stellar and circumstellar activity of α Eri (HD 10144), the brightest Be star in the sky. We present a thorough discussion of the fundamental parameters of the object for an independent determination of its rotational distortion. We used stellar atmosphere models and evolutionary tracks calculated for fast rotating early-type stars. If the star is a rigid rotator, its angular velocity rate is $\Omega/\Omega_c \simeq 0.8$, so that its rotational distortion is smaller than the one inferred from recent interferometric measurements. We then discuss the stellar surface activity using high resolution and high *S/N* spectroscopic observations of He I and Mg II lines, which concern a period of Hα line emission decline. The variations in the He I lines are interpreted as due to non-radial pulsations. Time series analysis of variations was performed with the CLEANEST algorithm, which enabled us to detect the following frequencies: 0.49, 0.76, 1.27 and 1.72 c/d and pulsation degrees $\ell \sim (3{-}4)$ for $\nu = 0.76$ c/d; $\ell \sim (2{-}3)$ for $\nu = 1.27$ c/d and $\ell \sim (3{-}4)$ for $\nu = 1.72$ c/d. The study of the absolute deviation of the He I λ6678 Å spectral line revealed mass ejection between 1997 and 1998. We conclude that the lowest frequency found, $\nu = 0.49$ c/d, is due to the circumstellar environment, which is present even at epochs of low emission in the wings of He I λ6678 Å and Mg II λ4481 Å line profiles, as well as during nearly normal aspects of the Hα line. This suggests that there may be matter around the star affecting some spectral regions, even though the object displays a B-normal like phase. The long-term changes of the Hα line emission in α Eri are studied. We pay much attention to the Hα line emission at the epoch of interferometric observations. The Hα line emission is modeled and interpreted in terms of varying structures of the circumstellar disc. We conclude that during the epoch of interferometric measurements there was enough circumstellar matter near the star to produce λ2.2 μm flux excess, which could account for the overestimated stellar equatorial angular diameter. From the study of the latest B⇌Be phase transition of α Eri we concluded that the Hα line emission formation regions underwent changes so that: a) the low Hα emission phases are characterized by extended emission zones in the circumstellar disc and a steep outward matter density decline; b) during the strong Hα emission phases the emitting regions are less extended and have a constant density distribution. The long-term variations of the Hα line in α Eri seem to have a 14–15 year cyclic B⇌Be phase transition. The disc formation time scales, interpreted as the periods during which the Hα line emission increases from zero to its maximum, agree with the viscous decretion model. On the other hand, the time required for the disc dissipation ranges from 6 to 12 years which questions the viscous disc model.

Key words. stars: emission-line, Be – stars: activity – stars: oscillations – stars: rotation – stars: fundamental parameters – stars: circumstellar matter

1. Introduction

Late O, all B sub-spectral types and early A-type non-supergiant stars that have shown at least once some emission in Balmer lines are considered to display the Be phenomenon (Jaschek et al. 1981). Be stars represent 17% of the B non-supergiant star population in our Galaxy, with a maximum frequency at B1–B2 spectral types (Zorec & Briot 1997). Among the most important characteristics of these stars is their fast rotation: $0.8 \lesssim \Omega/\Omega_c \lesssim 1.0$ (Chauville et al. 2001; Townsend et al. 2004; Frémat et al. 2005) and their spectroscopic and photometric variations, of which the most outstanding are the phase B⇌Be⇌Be-shell transitions. Phase transitions are revealed by the Balmer line emission intensity and global profile changes, as well as by changes in the visible energy distribution, mostly near the Balmer discontinuity (Moujtahid et al. 1998). These changes can be due either to variations of the physical structure and size of a more or less permanent circumstellar envelope (hereafter CE), or to the creation of a new CE during mass ejection events of the central star. The CE is assumed disk-like with Keplerian rotation (cf. Struve 1931; Marlborough 1976; Waters & Marlborough 1994; Hanuschik 1995). Interferometric and linear polarization measurements give some observational insights into the CE flattening (Gies et al. 1990; Stee et al. 1995; Quirrenbach et al. 1997; Yudin 2001; Tycner 2004). However, the inferred Keplerian rotation

⋆ Based on observations made at the MCT/LNA Observatory, Brasópolis – Brazil, and at ESO/La Silla – Chile and CASLEO operated under agreement between CONICET and National Universities of La Plata, Córdoba and San Juan, Argentina.

of the CE challenges our understanding, since it requires an amount of angular momentum that the surface of an even critically rotating star cannot provide alone.

Variations in the line profiles and continuum energy distribution are of short- (minutes to few days), intermediate- (weeks to months) and long-term (years to decades) (Porter & Rivinius 2003). The causes of short- to long-term line and flux variations can be of stellar and circumstellar origin. Authors like Vogt & Penrod (1983), Osaki (1986), Ando (1991), Rivinius et al. (1998, 2001), Floquet et al. (2000), Levenhagen et al. (2003), Štefl et al. (2003a) have made links between non-radial pulsations, periodic outbursts and temporal evolutions of CEs. On the other hand, the long-lived light outbursts (Guinan & Hayes 1984; Hanuschik et al. 1993, 1995, 1996; Hubert & Floquet 1998; Keller et al. 2002; Mennickent et al. 2002) have been interpreted by Moujtahid et al. (1999) and Hubert et al. (2000) in terms of discrete mass ejection with $\Delta M \sim 10^{-9}$–$10^{-10}\ M_{\odot}$.

The mechanisms related to winds and discrete ejections of mass and the acceleration of this mass into a Keplerian rotation to form the disc shaped CE are poorly understood. The processes involved in the creation of the CE may imply among others, mass-loaded wind-type interactions (Hartquist et al. 1986), viscous decretion (Porter 1999; Okasaki 2000) and magnetic acceleration (Balona 2000; Neiner et al. 2003). The importance of the fast rotation of Be stars in the formation of the CE has been put forward by Struve (1931), Stoeckley (1968), Owocki (2005) and Townsend et al. (2004). In a study of the effects due to the gravitational darkening on the measured $V \sin i$ parameters, Stoeckley (1968) suggested that Be stars might be critical rotators, so that "...mild prominence activity or other minor disturbances lead to the ejection of matter...". These arguments were taken up again by Owocki (2005) and Townsend et al. (2004). However, in a recent study of fundamental parameters of 130 Be stars, where detailed account is made of the gravitational darkening, Frémat et al. (2005) have shown that these objects rotate on average at an angular velocity ratio $\overline{\Omega/\Omega_{\rm c}} = 0.88$ within a small dispersion $1\sigma = 0.05$, so that only a small fraction of Be stars are in principle proper critical rotators. On the other hand, interferometric measurements of the brightest known Be star, α Eri, carried out by Domiciano de Souza et al. (2003), suggest that the star has a flattening exceeding the predicted one by a Roche model of a critical rigid rotator.

Since α Eri is the brightest Be star in the sky ($V = 0.46$ mag), a more detailed inquiry on the stellar characteristics can be carried out than in other Be stars.

The triggering of the Be phenomenon may be related to the structure and properties of fast rotating stars. The abovementioned interferometrically measured flattening of α Eri cannot be accounted for with models of rigid rotators. Although differential rotators with high internal content of angular momentum can produce the required flattening, they do not correctly reproduce the observed spectrum (Jackson et al. 2004). It is then important to inquire whether subtle perturbing circumstellar environments could mar the near-infrared (λ2.175 μm) interferometric measurements during apparently quiescent phases of the Be star in the visible spectral range and produce unexpected shapes of the projected stellar disc in the IR at λ2.2 μm. We have at our disposal spectroscopic observations over a period of relative low circumstellar emission of α Eri. In particular, we have Hα line emission profiles observed halfway through the epoch of interferometric measurements.

Therefore, two main questions motivate the present work:

a) what is the upper reliable limit of stellar deformation that can be inferred from spectroscopic, spectrophotometric and interferometric data consistent with the more advanced models of fast rotating stars;
b) can spectroscopic data reveal any stellar activity and presence of ejected matter near the star, which could mimic an apparent over-critical flattening of α Eri?

We divide the preset paper into three parts. Part I: determination of the stellar fundamental parameters (Sect. 3). This part is intended to discuss what stellar distortion better reconciles the latest interferometric results with the observed stellar spectrum and to obtain the rotational frequency that enable us to separate the spectroscopic short-term variations of stellar origin from those that may likely be of circumstellar nature. Part II: study of the α Eri spectroscopic activities and their relation to possible mass ejections at low Hα line emission phases (Sect. 4). This study investigates whether there are traces of matter flowing near the star that might introduce undesirable radiation excesses over the photospheric energy distribution. Part III: survey of the latest B$\rightleftharpoons$Be phase transition of α Eri using a model-dependent phenomenological description of the CE structures that govern the observed Hα line emission changes (Sect. 5). This part aims at giving quantitative estimates of the extent of the CE at each emission phase and the amount of pervasive, though elusive matter present around the star during or at near its B-normal like phases. In particular, we would like to give a quantitative estimate of the λ2.2 μm continuum flux excess possibly produced by the circumstellar matter at the epoch of interferometric observations.

2. Observations

Two type of data are used. The discussion of fundamental parameters is based on newly observed spectroscopic and BCD spectrophotometric data and on photometric/spectrophotometric flux measurements taken form the CDS database.

High resolution and high *S/N* spectra of the Be star α Eri for about 10 years were obtained, from November 1991 to October 2002. These observations total 510 spectra that cover a significant part of the B$\rightleftharpoons$Be activity cycle of this star. From Nov. 1991 to Dec. 1995 only the Hα line was observed. From Nov. 1997 to Oct. 2002 several He I lines, as well as the Hα line were observed. Observations were carried out at the Laboratório Nacional de Astrofísica at Pico dos Dias (Brazil) with the coudé spectrograph installed in the 1.60 m B and C telescope with an EMI CCD camera (1152×770 pixels). We used an 1800ℓ/mm dispersion grating (first inverse order), centered at He I λ6678 Å plus one or two spectra of the Hα line per night. The spectral resolution is $R \sim 40\,000$ with a reciprocal dispersion of 0.08 Å/pixel over a coverage of 90 Å. The

Table 1. Log of spectroscopic observations of α Eri.

Epoch	Site	Number of spectra	Range or individual spectral lines		
Nov. 1991	LNA/Brazil	4	Hα	–	–
Aug.–Oct. 1993	LNA/Brazil	3	Hα	–	–
Nov. 1994	LNA/Brazil	1	Hα	–	–
Nov.–Dec. 1995	LNA/Brazil	3	Hα	–	–
Nov. 1997	LNA/Brazil	169	–	He I 6678 Å	–
Nov.–Dec. 1998	LNA/Brazil	118	Hα	He I 6678 Å	–
Oct. 1999	ESO/Chile	123	from 3600 until 8500 Å		
Oct. 2000	LNA/Brazil	89	Hα	He I 6678 Å	Mg II4481 Å
Sep.–Oct. 2002	LNA/Brazil	3	Hα	–	–

typical *S/N* ratio is ∼200 for exposure times ∼100 s. The suitable corrections for bias, flat field, heliocentric velocity and wavelength calibration with a Th-Ar lamp were made using the IRAF[1] software package. The 1999 season spectra were obtained with the fiber-fed extended range optical spectrograph (FEROS) at the ESO – La Silla 1.52 m telescope (Chile). The ESO spectra have a coverage of about 4900 Å (from ∼3600 to ∼8500 Å) with a spectral resolution $R \sim 48\,000$ and typical *S/N* ratios ∼300. We note, however, that in the He I λ6678 region of FEROS spectra there is a flaw in the CCD detector (private communication from the ESO technical staf) which cannot be eliminated entirely by the reduction procedure. So, this line has not been used in the present paper to obtain information on the stellar and circumstellar activity of α Eri during our 1999 observing run. The log of spectroscopic observations is shown in Table 1, with the observing seasons and the number of spectra obtained each night.

α Eri was observed in the spectrophotometric BCD system (Chalonge & Divan 1952) from 3 to 12 Oct. 1979 at ESO (La Silla, Chile) with the Chalonge spectrograph (Baillet et al. 1973) and on 3 Sep. 2004 in CASLEO (San Juan, Argentina) with the Booller & Chivens Cassegrain spectrograph, whose resolution in the low dispersion mode is similar to that of the Chalonge spectrograph (Cidale et al. 2001). The low resolution spectra are for the $\lambda\lambda$ 3200–6400 Å, or $\lambda\lambda$ 3500–5400 Å spectral regions. The usefulness of this system for Be stars was discussed in Zorec & Briot (1991). From the photospheric component of the Balmer discontinuity, unperturbed by the circumstellar emission/absorptions and ISM extinction, we determine two quantities: D, the flux jump given in dex at $\lambda = 3700$ Å and λ_1 given in $\lambda - 3700$ Å, which is the average spectral position of the Balmer discontinuity. In Table 2 we give the values of the photospheric (λ_1, D) parameters of α Eri.

3. The central star

α Eri or Achernar (HD 10144, HR 472, SAO 232481) is the brightest Be star in the sky. Its Be nature was established by Andrews & Breger (1966) when they found a strong emission in the Hα line. The spectral type attributed in the literature to the central star ranges from B3IV (Hiltner et al. 1969), B4V (Slettebak 1982) to B3-B4III (Balona et al. 1987). From the photometric data corresponding to an emissionless phase, bolometric correction calibrations and the HIPPARCOS parallax of α Eri, Harmanec (2000) obtained $T_{\rm eff} = 14\,500$ K, $\log L/L_\odot = 3.518$ and $R_*/R_\odot = (9.01\text{–}9.10) \pm 0.55$ that likely corresponds to a MK spectral type B5III. Using the (λ_1, D) calibration in MK spectral types (Chalonge & Divan 1973) we obtain B4III.

The determination of fundamental parameters from models for rotating stars needs a thorough discussion of quantities derived from observations. To be sure of their reliability, we redetermined the fundamental parameters of α Eri using several different methods.

3.1. Three types of fundamental parameters

Quantities like $T_{\rm eff}$, $\log L/L_\odot$, $\log g$ and $V\sin i$ of rotating stars derived either by adjusting the observed spectral lines and energy distributions with model atmospheres calculated for non-rotating objects, or comparing with calibrations where rotation is not taken into account, will be called hereafter "*apparent*" fundamental parameters. They "summarize" the characteristics of a rotationally distorted and the temperature and gravity non-uniform aspect-angle-dependent observed stellar hemisphere.

The atmosphere models of rotating stars used are from Frémat et al. (2005), which are parametrized in terms of "*non-rotating parent counterpart*" fundamental parameters that correspond to objects of the same mass as the studied ones, but without rotation. We will use the acronym *nrpc*-parameters. From the same models we obtain a $V\sin i$ parameter corrected for underestimations carried by the gravitational darkening effect (Stoeckley 1968; Townsend et al. 2004; Frémat et al. 2005), which will be considered as the *true* $V\sin i$ of the star.

Evolutionary tracks calculated for rotating objects are presented in terms of $\log \overline{L/L_\odot}$ and $\overline{T_{\rm eff}}$ averaged over the whole rotationally deformed and gravitationally darkened stellar surface. From the *nrpc*-parameters we derive then the surface "*averaged*" quantities that enable us to evaluate the stellar mass and its age from evolutionary models with rotation.

The names of parameters given above are from Frémat et al. (2005) and Zorec et al. (2005), where the models of rotating stars used in the present paper are presented.

[1] IRAF is distributed by the National Optical Astronomy Observatories, which is operated by the Association of Universities for Research in Astronomy (AURA), Inc., under cooperative agreement with the National Science Foundation.

Table 2. Fundamental parameters of α Eri.

BCD parameters			
$\lambda_1 =$	39.9 ± 0.5 Å		
$D_* =$	0.241 ± 0.008 dex		
$T_{\rm eff} =$	15 044 ± 300 K		
$\log g =$	3.48 ± 0.05		
$\log L/L_\odot =$	3.488 ± 0.110		
$R/R_\odot =$	8.2 ± 0.60		
Parameters from fluxes		Interferometry	
$T_{\rm eff} =$	15 000 ± 200 K		
$\theta =$	1.84 mas	$\theta =$	1.85 mas
$\log L/L_\odot =$	3.542 ± 0.080	$R_{\rm p}/R_\odot =$	7.7 ± 0.2
$R_{\rm sph}/R_\odot =$	8.7 ± 0.4	$R_{\rm e}/R_\odot =$	12 ± 0.4
Parameters from spectroscopy			
$T_{\rm eff} =$	15 000 ± 200 K		
$\log g =$	3.45 ± 0.10 K		
H/He =	0.12 ± 0.05		
$V \sin i =$	223 km s^{-1}		

The (λ_1, D) parameters of O and B stars were calibrated in $T_{\rm eff}$, $\log g$ and $\log L/L_\odot$ determined empirically, but without considering rotation-induced changes (Divan & Zorec 1982; Zorec 1986). They were also modeled for non-rotating and rotating stars (Zorec et al. 2005). The *apparent* fundamental parameters derived from these calibrations and models are given in the 1st block of Table 2.

The continuum energy distribution of α Eri was observed in the spatial UV, in the visible spectral range and in the near- and far-IR wavelengths. The fluxes used correspond to a low, if any, emission phase in the Hα line. To calculate the effective temperature and the stellar angular diameter, as if it were an emissionless B-normal star, we used the definition of $T_{\rm eff}$:

$$\left.\begin{array}{rcl} T_{\rm eff}^4 & = & 4f/\sigma\theta^2 \\ \theta & = & 2\,(f_\lambda/F_\lambda)^{1/2} \end{array}\right\} \quad (1)$$

where f is the flux received on Earth corrected for ISM extinction and integrated over the full extent of the spectrum, σ is the Štefan-Boltzmann constant, θ is the angular diameter of the star, f_λ is the absolute monochromatic flux received on Earth corrected for ISM extinction and F_λ is the absolute monochromatic flux emitted by the star. f was determined using several spectrophotometric measurements calibrated in absolute fluxes: (far-UV) Skylab (Henize et al. 1975), TD-1 satellite (Jamar et al. 1974), ANS satellite (Wesselius et al. 1982) and IUE satellite (CDS database); (visible) 13-color photometry of Johnson & Mitchell (1975) calibrated in absolute fluxes, Kaiser (1989), Dachs et al. (1989); near-IR (Alonso et al. 1994), (far-IR) IRAS satellite (CDS database). These fluxes were compared and discussed in order to obtain the most reliable energy distribution corresponding to a non-emission phase. This phase is well depicted by the measurement carried out at the epoch of the 13-color photometry and the TD-1 and Skylab fluxes. We used $E(B-V) = 0.0$ as the star is not far from the Sun. The wavelength interval used to determine θ ranges from $\lambda\lambda$ 0.5 to 0.7 μm. The fluxes F_λ and those employed to complete f in the non-observed spectral regions ($\lambda\lambda$ 0–1200 Å and 100 μm-∞ are from Kurucz' (1994) LTE non-rotating model atmospheres. We iterated $T_{\rm eff}$ and θ in relation (1) until two consecutive steps produced differences $\delta T_{\rm eff} \lesssim 1$. The $\delta T_{\rm eff}$ is the tolerance in each iteration which gives the difference accepted or intrinsic error carried by the iteration procedure. The total error affecting the $T_{\rm eff}$ determination depends on the flux measurement errors, the fitting errors at the fluxes where θ is calculated and possible uncertainties on $E(B-V)$ around the adopted value. They all amount roughly to ±200 K. The values of $T_{\rm eff}$ and θ thus obtained are given in the 2nd block of Table 2.

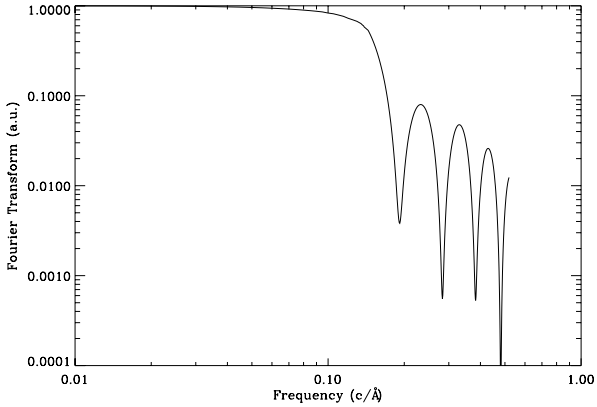

Fig. 1. Fourier transform of the observed He I λ4471 Å line profile.

3.2. Rotational velocity

We estimated the projected rotation velocity $V \sin i$ using the Fourier transform of the He I λ4471 Å line profile (Gray 1992). The estimated $V \sin i = 223 \pm 15$ km s^{-1} was obtained from the first zero of Fourier transform (Fig. 1). We assumed a quadratic limb-darkening law of the continuum for the rotation broadening function (Wade & Rucinski 1985). The corresponding limb-darkening coefficients were obtained using the $T_{\rm eff}$ and $\log g$ parameters inferred in Sect. 3.1. Our $V \sin i$ determination is somewhat lower than obtained by Chauville et al. (2001) where the models used take into account the variation of the limb-darkening coefficient with wavelength within the spectral line He I 4471. The underestimation can then be due to effects carried by the use of a constant limb-darkening coefficient (Collins & Truax 1995). So, in order to determine the effects carried by the fast rotation, we used Chauville's et al. (2001) $V \sin i = 235$ km s^{-1}. However, the fits of spectra to obtain *apparent* stellar parameters were performed by broadening the spectral lines with $V \sin i = 223 \pm 15$ km s^{-1}, since the broadening function is constructed with limb-darkening coefficients that are constant in the wavelengths within the line profiles.

3.3. Fundamental parameters derived from spectroscopy

Using the code SYNSPEC (Hubeny 1994) from TLUSTY non-LTE model stellar atmospheres (Hubeny 1990) for non-rotating

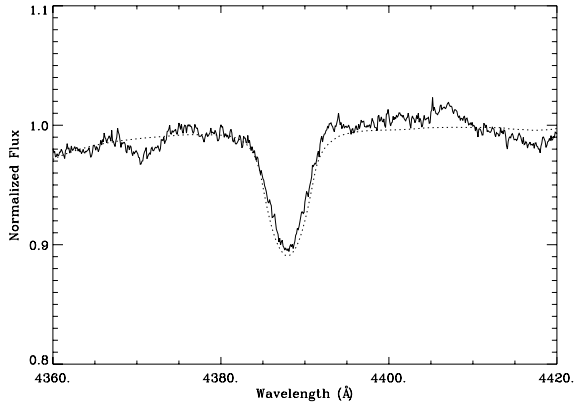

Fig. 2. Full line: observed spectrum of α Eri in the He I λ4388 Å line region. Dashed line: model spectrum for $T_{\rm eff}$ = 15 000 K and $\log g$ = 3.30 dex, broadened with $V \sin i$ = 223 km s^{-1}.

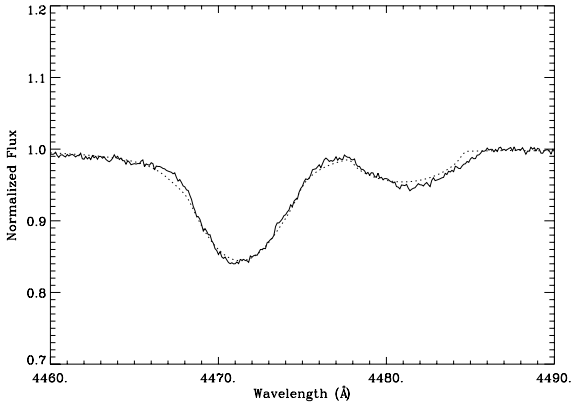

Fig. 3. Same as Fig. 2, but for the He I λ4471 Å and Mg II λ4481 Å line profiles. The He I λ4471 Å was used to determine $V \sin i$ = 223 km s^{-1} with the Fourier transform method.

stars, we generated a grid of synthetic spectra for $T_{\rm eff}$ values in the range 15 000–2000 K by steps of $\Delta T_{\rm eff}$ = 100 K, gravity parameters $2.0 \leq \log g \leq 5.0$ dex with steps $\Delta \log g$ = 0.1 dex and He abundance in number ratios $0.01 \leq$ (He/H) ≤ 0.3 spaced by Δ(He/H) = 0.05. As noted in Sect. 3.2, we fitted with them the He I $\lambda\lambda$ 4388, 4471, 4922 Å lines, where the model line profiles were broadened with $V \sin i$ = 223 km s^{-1} issued from the Fourier method. The fitting procedure included a χ^2 test. The most reliable fit of the helium lines was achieved with the parameters given in the 3rd block of Table 2. In Figs. 2–4 are shown the fits thus obtained of the observed He I $\lambda\lambda$4388, 4471, 4922 Å and Mg II λ4481 Å line profiles. Figure 3 shows the fit of the He I 4471 line that was used to determine the $V \sin i$ parameter.

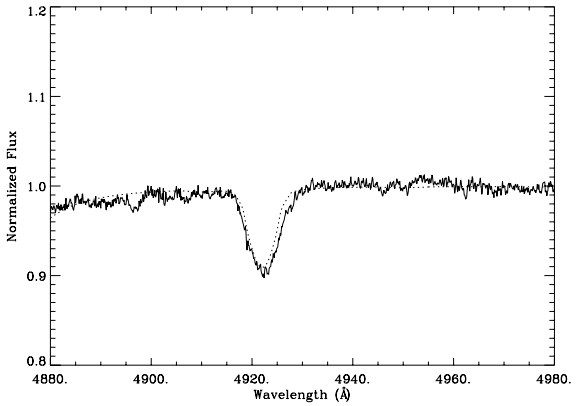

Fig. 4. Same as Fig. 2, but for the He I λ4922 Å line profile.

3.4. Consistency requirements

Our determination of θ from absolute fluxes is in excellent agreement with the measured angular diameter of α Eri by Hanbury Brown et al. (1974): θ = 1.85 ± 0.07 mas, which supports the $T_{\rm eff}$ determined from f and the estimate of the average (circular) stellar diameter. We note that the measurements of θ were carried out in October 1965 during a phase of Hα line emission (Andrews & Breger 1966). However, they were performed in λ4385 where the photospheric continuum flux of α Eri is not perturbed by the circumstellar radiation. In stars like α Eri, the Hα line emission must be stronger than observed for there to be a flux excess in the visual continuum produced by the circumstellar matter (Moujtahid et al. 1999). This may not be the case for the far-IR spectral region (Kogure & Hirata 1982). This issue is discussed in Sect. 5.4.

From the angular diameter θ and the HIPPARCOS parallax of α Eri (distance $d_{\rm Hipp} = 44.1^{+1.1}_{-1.2}$ pc, Perryman et al. 1997) we derived the radius $R_{\rm sph}$ of the "equivalent" circular stellar disc projected onto the sky. With this distance and the distance-reduced bolometric flux f we calculated the bolometric luminosity $\log L/L_\odot$ of α Eri used in the next sections. These quantities are given in the 2nd block of Table 2. The $R_{\rm sph}$ derived from absolute fluxes is the same, within measurement uncertainties, as the visual interferometric one. If visual and far-IR interferometric measurements refer to the same average photosphere, the area of the equivalent circular projection of the star onto the sky ($\pi R^2_{\rm sph}$) and the area of the projected "Roche-shaped" stellar surface (very nearly an ellipse: $\pi R_{\rm p}^{\rm interf} R_{\rm e}^{\rm interf}$) must be the same within measurement uncertainties. However, from the values in Table 2 we can see that these areas differ by more than 20%.

The transformation of interferometric "visibilities" into angular diameters in regions that likely correspond to the stellar equator reveals larger error bars than in other stellar latitudes. This might have thwarted a better determination of the equatorial radius. Due to these difficulties, we would like to know what the stellar shape is that better reconciles the *apparent* fundamental parameters displayed in Table 2 and the interferometric measurements, under the assumption that the star is a rigid fast rotator.

3.5. Actual shape of α Eri

Be stars rotate on average at an angular velocity ratio close to $\Omega/\Omega_{\rm c} \sim 0.9$ (Frémat et al. 2005). The stellar geometrical distortion and the concomitant gravitational darkening are then non negligible. Assuming the star is a rigid rotator, the ratio between the equatorial $R_{\rm e}(\omega)$ and the polar $R_{\rm p}(\omega)$ radii predicted by a Roche model surface equipotential is:

$$\frac{R_{\rm e}(\omega)}{R_{\rm p}(\omega)} = 1 + \frac{1}{2}\omega^2 \left[\frac{R_{\rm e}(\omega)}{R_{\rm c}}\right]^3, \qquad (2)$$

where $\omega = \Omega/\Omega_c$ is the ratio of the stellar angular velocity to its critical one; R_c is the critical equatorial radius. For critical rotation ($\omega = 1$), relation (2) yields:

$$R_e(\omega=1) = 1.50 R_p(\omega=1), \quad (3)$$

while from the interferometric measurements carried out by Domiciano et al. (2003):

$$R_e^{interf} = (1.56 \pm 0.05) R_p^{interf}, \quad (4)$$

that within 1σ uncertainty might represent a critical rigid rotator in the Roche approximation. Domiciano et al. (2003) state, however, that the measured flattening corresponds to an apparent stellar uniform bright disc seen at an aspect angle $i < 90°$, so that the actual polar radius can be smaller than the measured one. In this case, the obtained radii ratio can imply either an over-critical deformation of the star, or that the object rotates with a total angular momentum higher than allowed for rigid rotators, which implies a non negligible degree of internal differential rotation (Jackson et al. 2004). Concerning relation (3) we note that $R_p(\omega=1)/R_o < 1$ (Frémat et al. 2005), where R_o is the radius a rotationless star with the same mass.

Using Frémat's et al. (2005) models for fast rotating stars and the quantities T_{eff}, $\log g$ or $\log L/L_\odot$ and $V \sin i$ given in Table 2 as entry parameters, for a given set of parametrized rotational rates ω, we derived the corresponding *nrpc* effective temperature, gravity or luminosity and the *true* $V \sin i$, i.e. the projected rotational velocity corrected for underestimations due to the gravitational darkening effect. The procedure also requires one to interpolate the stellar mass in a theoretical HR diagram for rotating objects (Zorec et al. 2005). The method provides us with $i(\omega)$, $R_e(\omega)$ and $R_p(\omega)$ for each rotation rate ω, which are not new independent quantities, but are dependent on ω that are related to the *nrpc*-parameter determination. They all are given in Table 3. The translation from *apparent* to *nrpc*/*true* parameters operates as we had three conditions/equations with four independent variables, where the rotation rate ω is one of them. In order to have the system of conditions complete to derive the stellar ω_*, we used the additional independent closure requirement, given by the interferometric determination of the stellar polar radius. Due to the activity of α Eri and its expected high rotation rate ω_*, the equatorial stellar regions can be rather unstable and strongly perturbed. We assume then that the polar region of the star is less affected by activity than the equator and seek a correspondence between the model $R_p(\omega)$ values of Table 3 and the measured one: $R_p^{interf} = 7.7\ R_\odot$. However, if the star is seen at an inclination angle $i < \pi/2$, the measured value R_p^{interf} does not reflect the polar radius directly, but the semiminor axis of an ellipse representing the stellar disc projected onto the sky, as shown in Fig. 5, which is larger than the actual stellar polar radius. The projected model polar radii $R_p^{app}(\omega)$ were calculated using the Roche representation of the stellar surface deformation, although the relation between R_p and R_p^{app} is given by:

$$\frac{R_p^{app}(\omega)}{R_e(\omega)} \simeq \left\{ 1 - \left[1 - \left(\frac{R_p(\omega)}{R_e(\omega)} \right)^2 \right] \sin^2 i \right\}^{\frac{1}{2}}. \quad (5)$$

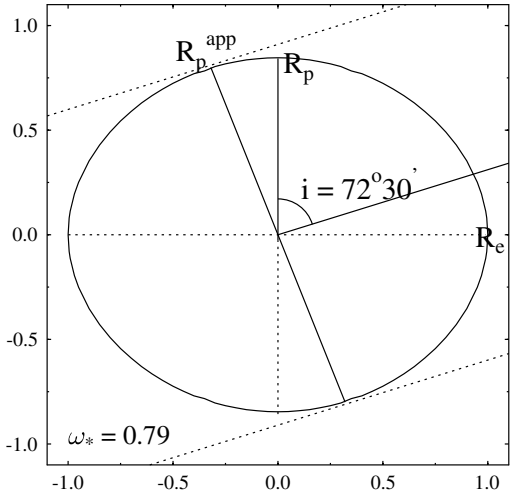

Fig. 5. Meridional cut of the Roche-shaped star at $\omega = 0.79$ seen at $i = 72.5°$. Polar actual R_p and the aspect angle-dependent apparent polar R_p^{app} radii are shown.

So, making $R_p^{app}(\omega) = R_p^{interf}$, we interpolated in Table 3 the polar radius R_p which hence identify the sought solutions: $\omega_* = 0.79$ and $i(\omega_*) = 72.5°$.

Contrary to expectations, the value of ω_* is smaller than the average found by Frémat et al. (2005) for the Galactic Be star population. This supports the idea that the Be phenomenon does not require the stars necessarily to be critical rotators.

The set of *true* $V \sin i$, i, R_e and R_p model parameters corresponding to $\omega_* = 0.79$ are boldfaced in Table 3. Since the inclination is rather high, $R_p^{app} \simeq R_p$. On the other hand, the "true" stellar flattening becomes: $R_e/R_p = 9.0/7.6 = 1.2$, which is much smaller than the measured one (4).

Before discussing the possible effects that may mar the measurements that lead to $R_e^{interf} = 12 > 9 = R_e(\omega_*)$, we comment the interpretation of equatorial and polar radii from arguments based on averaged apparent surface quantities.

3.6. Apparent stellar distortion

The distance-reduced bolometric flux f obtained in Sect. 3.1 can be rewritten for a rotationally deformed star as:

$$\left. \begin{array}{rcl} f & = & \frac{\int_{\mathcal{S}(i,\omega)} \sigma T_{eff}^4(s) \mathrm{d}s}{4\pi d^2} \\ & = & \frac{\phi(i,\omega)}{4\pi} \left[\frac{R_e(\omega)}{d} \right]^2 \sigma \left\langle T_{eff}^4(\mathcal{S}) \right\rangle \end{array} \right\}, \quad (6)$$

where $R_e(\omega)$ is the equatorial radius; $\langle T_{eff}^4(\mathcal{S}) \rangle$ is the average effective temperature of the observed stellar hemisphere; $\mathcal{S}(\omega, i)$ is the observed stellar surface; d is the stellar distance and $\phi(i, \omega) \lesssim 4\pi$ is a value obtained from numerical integration of Eq. (6), where $T_{eff}(s)$ is assumed to be given by the von Zeipel's (1924a,b) gravity darkening law. In order to approach the observed R_e^{interf} and R_p^{interf} values with the theoretical ones R_e and R_p^{app} as closely as possible, let us assume the extreme situation, i.e. the star being seen equator-on and rotating at the critical rigid rotation. From Eq. (6) it is:

$$R_e(\omega)^2 = \frac{R_{sph}^2}{(\phi/4\pi)} \frac{T_{eff}^4}{\left\langle T_{eff}^4(\mathcal{S}) \right\rangle}. \quad (7)$$

Table 3. Parameters of α Eri derived from models of rotating stars.

	nrcp-parameters			*true*-parameters			
ω	$T_{\rm eff}$	$\log g$	$\log L/L_\odot$	$V \sin i$	i°	$R_{\rm e}$	$R_{\rm p}$
0.00	**15 000**	**3.47**	**3.542**	**235**	–	**8.73**	**8.73**
0.70	16 119	3.63	3.624	238	39.9	8.96	8.01
0.75	16 240	3.64	3.623	240	57.3	8.99	7.84
0.80	16 385	3.65	3.614	243	76.3	8.95	7.58
0.85	16 559	3.65	3.600	247	66.0	8.88	7.25
0.90	16 763	3.65	3.580	255	59.0	8.76	6.85
0.95	17 001	3.64	3.553	267	52.8	8.57	6.36
0.99	17 218	3.62	3.528	282	52.5	8.63	5.98
1.00	17 276	3.62	3.521	286	50.0	8.78	5.86
ω_*	*nrcp*-parameters			*true*-parameters			
0.79	16 356	3.65	3.616	**242**	**72.5**	**8.96**	**7.63**
	surface *averaged*			$\frac{M}{M_\odot}$	$\log \tau$ (yr)	$\frac{\tau}{\tau_{\rm MS}}$	$\nu_{\rm rot}$ c/d
	16 090	3.47	3.510	**6.73**	**7.74**	**0.96**	**0.57**

The integration of Eq. (6) for $i = \pi/2$ and $\omega = 1.0$ produces $\phi_1/4\pi = 0.6$. If we assume, as it was done in the reduction of interferometric data, that $\langle T_{\rm eff}^4(\mathcal{S})\rangle = T_{\rm eff}^4$ = the *apparent* effective temperature given in Table 2, then:

$$\left.\begin{array}{rcl} R_{\rm e}^{\rm c} & = & 1.3 R_{\rm sph} = 11.3 \pm 0.5\ R_\odot \\ R_{\rm p}^{\rm c} & = & R_{\rm e}^{\rm c}/1.5 = 7.6 \pm 0.3\ R_\odot \end{array}\right\} \quad (8)$$

that within the measurement uncertainties approach quite closely the interferometric determinations by Domiciano de Souza et al. (2003). However, it can be shown that $\langle T_{\rm eff}(\mathcal{S})\rangle \lesssim 16\,000$ K, while the *apparent* $T_{\rm eff} = 15\,000$ K, which significantly reduces the values of both $R_{\rm e}^{\rm c}$ and $R_{\rm p}^{\rm c}$ and tends to argue against a large equatorial radius. While the apparent effective temperature seems to act as an average parameter, it actually defines an aspect angle average spectrum, but not a surface mean effective temperature over the observed hemisphere.

Radii given in Eq. (8) also fail to obey the area conservation requirement discussed in Sect. 3.4. Conversely, using the values of Table 3 we obtain $[R_{\rm e}(\omega_*)R_{\rm p}^{\rm app}(\omega_*)]^{1/2} = 8.3\ R_\odot$, which is close to $R_{\rm sph} = 8.7\ R_\odot$.

We may ask whether one or both interferometric radii are marred by effects due to stellar activities and/or possible ejected matter orbiting close to the star at the measurement epochs. Noting that the estimated inclination of the star is rather high ($i \gtrsim 70^\circ$), matter spread in the equatorial region will hardly affect the measurement of $R_{\rm p}^{\rm app}$.

3.7. Mass, evolutionary stage and the rotational frequency

For completeness we also derive the mass, age (τ), fraction of age in the main sequence ($\tau/\tau_{\rm MS}$) and the rotational frequency of α Eri. From the *nrpc*-parameters we derive the surface *averaged* ones $\overline{T_{\rm eff}}$ and $\log \overline{L/L_\odot}$ using the method described in Zorec et al. (2005), which enable us to interpolate in the evolutionary tracks with rotation calculated by Meynet & Maeder (2000). The so-derived quantities are given in the last block of Table 3. The high value of $\tau/\tau_{\rm MS}$ obtained indicates that the star is near the end of its main sequence evolutionary phase.

The rotational frequency in c/d given in Table 3 was obtained with $\nu_{\rm rot} = 0.02 V_{\rm e}(\omega_*)/R_{\rm e}(\omega_*)$. This frequency will help us in Sect. 4.2 to distinguish the circumstellar activities from the stellar proper.

Finally, the critical equatorial velocity and the associated frequency are: $V_{\rm c} = 374$ km s^{-1}; $\nu_{\rm c} = 0.85$ c/d.

4. Short-term stellar and circumstellar activities

α Eri presents short-term spectral line profile variations which, nevertheless, are difficult to measure because of their low amplitude (lower than 1% of the continuum). The star is classified as a ζ Oph variable-type star, since it is a rapidly rotating pulsating star with $V \sin i \gtrsim 170$ km s^{-1} (Unno et al. 1989).

The aim of the next sections is to perform a thorough time series analysis of spectral line variations to detect frequencies that cannot be due to photospheric activity, but possibly to nearby ejected mass. We shall study spectra which unfortunately are not simultaneous with the interferometric data. However, there are some data that correspond to an apparent "absolute" minimum of circumstellar activity. Any detection of circumstellar activity in this epoch is then important, because at the epoch of interferometric observations, the star did not show obvious spectral emission signatures. The presence of such "elusive" matter may account for the apparently oversized stellar equatorial radius derived interferometrically. As we look for circumstellar signatures of activity in He I lines, the matter producing them should be close to the star in order to have enough temperature to excite the ion. On the other hand, in these environments the ff+bf optical depth in the photometric K-band wavelengths is roughly 10 times stronger than in the visual wavelength range (Kogure & Hirata 1982). This ensures that the 2.2 μm radiation is perturbed by emission in the circumstellar matter, while no noticeable effects will be present in the visible continuum radiation.

4.1. Short-term lpv

We have studied the short-term line profile variations (lpv) of α Eri in four He I lines: $\lambda\lambda$ 4388, 4471, 4922 and 6678 Å. We also analyzed the Mg II λ4481 line observed in Oct. 1999. The excitation potential of the lower levels of He I lines is about 21 eV, which is higher than the average exciting thermal energy in the CE, so that they could be considered of photospheric origin. However, among these He I lines the λ6678 Å has the highest $\log gf$ value. This can make the line more easily perturbed by circumstellar contributions than the remaining He I lines studied here. The lower level of the Mg II λ4481 line has a much smaller excitation potential, 8.8 eV, and its $\log gf$ is three times larger than that of He I λ6678. The Mg II line can then be easily perturbed by the emission/absorption of circumstellar origin. Thus, the He I $\lambda\lambda$4388, 4471 and 4922 lines have been considered as signs of photospheric activity, while

Table 4. Detected frequencies whose significance levels (statistical reliability) are higher than 70% and pulsation degrees ℓ. The uncertainties shown here are the values at half maximum of each frequency. The frequencies marked with an asterisk are considered to be aliases.

Frequency c/d	Significance	ℓ
0.49 ± 0.04	92%	
0.76 ± 0.09	97%	3–4
1.27 ± 0.12	90%	2–3
1.72 ± 0.15	80%	3–4
2.32* ± 0.10	72%	
3.30* ± 0.20	72%	

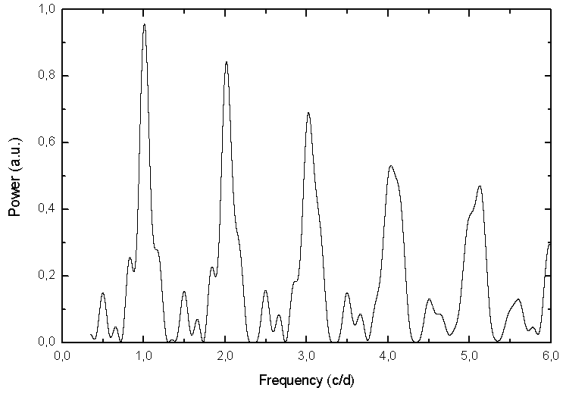

Fig. 6. Window functions of radial velocity for the He I and Mg II line group.

the He I λ6678 and Mg II λ4481 lines as carrying information related to the activity in the CE regions near the star (Štefl et al. 2003b). Although the Fe II λ5169 and Si II λ6347 Å lines were also frequently studied in the NRP frame (Rivinius et al. 1998; Levenhagen et al. 2003), which enter the FEROS spectral domain and can also carry information on the circumstellar activity, they are not present in our spectra.

4.2. Stellar and circumstellar pulsation frequencies and mode determination

Time series analysis of line variations were carried out using the Fast Fourier Transform (FFT) with the CLEANEST algorithm (Foster 1995). This method treats the temporal series as vectors that are decomposed on a vectorial base. Using an iterative process, the algorithm sequentially select the most convenient frequencies for the model functions of the data vectors. The procedure also analyzes the statistical significance of each frequency with a χ^2 test (Emílio 1997; Levenhagen et al. 2003).

Temporal analyses were performed on several line data sets: three of them correspond to the 1997+1998+2000 epoch, where for 1997 and 1998 we have He I λ6678 line profiles; four sets of the 1999 epoch are for the He I $\lambda\lambda$4388, 4471, 4922 and the Mg II λ4481 Å line profiles. The detected frequencies are given in Table 4. The window functions of radial velocity for the He I and Mg II line group is presented Fig. 6. The periodogram for all time series studied in this work is shown in the left panel of Fig. 7. In the right panel of Fig. 7 is reproduced the periodogram of the He I λ6678 Å corresponding to the 1997 epoch, to illustrate the corresponding frequencies detected in this line. Note that for the 1997 epoch, the time span covered by the data does not enable us to detect frequencies lower than 1 c/d.

In previous photometric and spectroscopic campaigns, Balona et al. (1987) found a variability of 0.79 c/d with amplitude of 0.02 mag in both radial velocity and light variation. Leister et al. (2000) also confirm the presence of this frequency and another three: 1.36, 1.90 and 2.60 c/d detected in the He I λ6678 Å line, where the last one is much less reliable. Recently, Rivinius et al. (2003) have reported the 1.29 c/d frequency, which is close to one of ours.

Since from Sect. 4.2 we know that the rotational frequency of the star is $\nu_{\rm rot}$ = 0.57 c/d, the 0.49 c/d frequency may correspond to some nearby CE activity. The 0.49 c/d frequency was present in the He I λ6678 Å line profiles from 1997 to 1999, which according to Fig. 15 correspond to a period in which the star underwent a Be→B phase transition. On the other hand, in the Mg II 4481 only one outstanding frequency was detected: ν = 0.49 c/d. This line is easily perturbed by emission/absorption effects due to circumstellar matter. We can conclude then that the 0.49 c/d frequency reveals the presence of circumstellar matter even during the 1999 epoch, which is an apparent Hα emissionless phase.

The 0.76, 1.27 and 1.72 c/d frequencies were seen in all epochs, so that they can be considered as due to NRP. Although the 2.32 and 3.30 c/d are seen with a high confidence level ($\gtrsim$70%), they may be aliases of the 1.27 c/d frequency.

We considered the 0.76, 1.27 and 1.72 c/d frequencies as the fundamental NRPs of the star and constructed for them the corresponding phase diagrams that are shown in Fig. 8. Using the IPS method of Telting & Schrivers (1997a,b,c) we obtained the pulsation degrees ℓ that are also presented in Table 4. The uncertainties in ℓ values calculated by this method are roughly $\epsilon_\ell \pm 1$. The amplitude profiles shown in Fig. 8 are characteristic of g-modes (Leister et al. 2000).

4.3. The He I λ6678 line profile changes

The He I λ6678 line was observed in four different epochs (see Table 1) of which one of them unfortunately gave non exploitable spectra (Oct. 1999); i.e. the blue wing of the line profile could not provide reliable measurements. According to a vertical time spacing, Fig. 9 displays the obtained nightly averaged He I λ6678 line profiles. The 1997-epoch averaged line profile shows noticeable deformations in the inner spectral regions at $|RV| \lesssim 200$ km s^{-1}. These deformations are almost completely washed out in the line profiles of the 1998-epoch, but the emission shoulders, centered roughly at $|RV| \simeq 300$ km s^{-1}, are clearly seen in both wings. The average line profile of the 2000-observation night has neither any apparent emission nor clearly developed internal asymmetry. We assumed that the 2000-year He I λ6678 average line profile

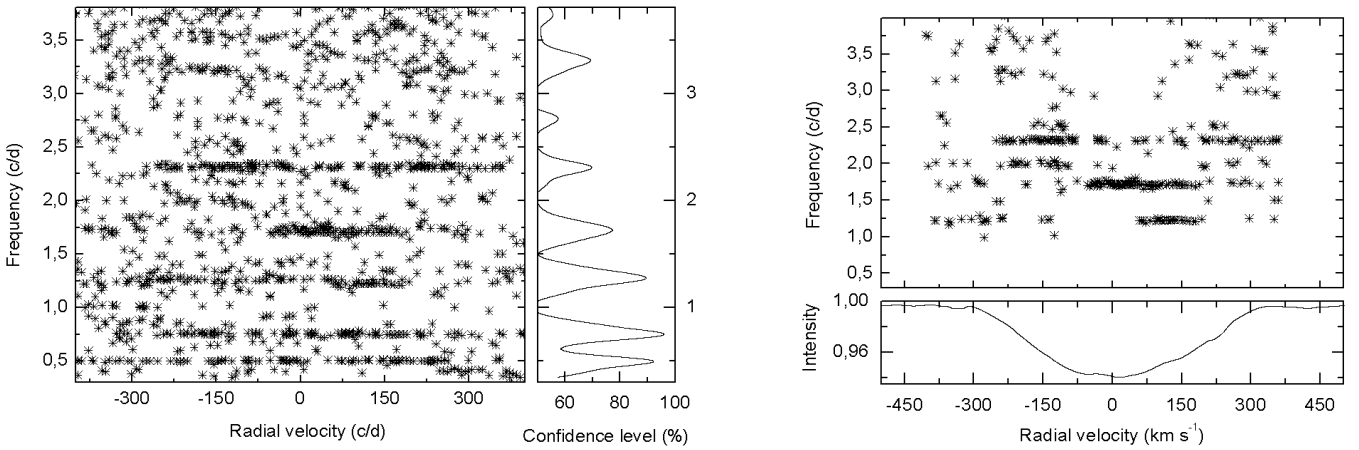

Fig. 7. *Left panel*: periodogram for all time series from 1997 until 1999. On the right side is the diagram of confidence levels. The frequencies discussed in this work are those whose confidence level is higher than 70%. *Right panel*: periodogram for the He I λ 6678 Å time series obtained during the 1997 LNA epoch. The respective mean line profile is showed in the bottom.

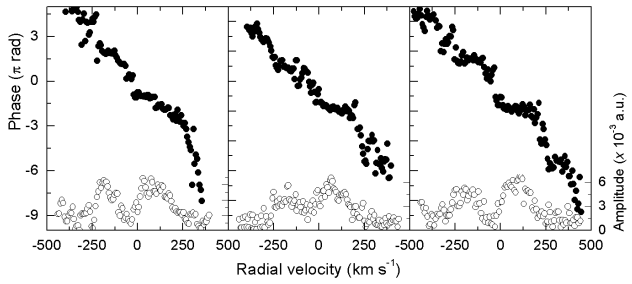

Fig. 8. IPS diagrams for the detected fundamental frequencies, *from left to right*: 0.76, 1.27 and 1.72 c/d. The filled circles show the phase diagram across the line profile. The amplitude of signals are represented by open circles. The phase scale is displayed on the left and the amplitude scale is displayed on the right.

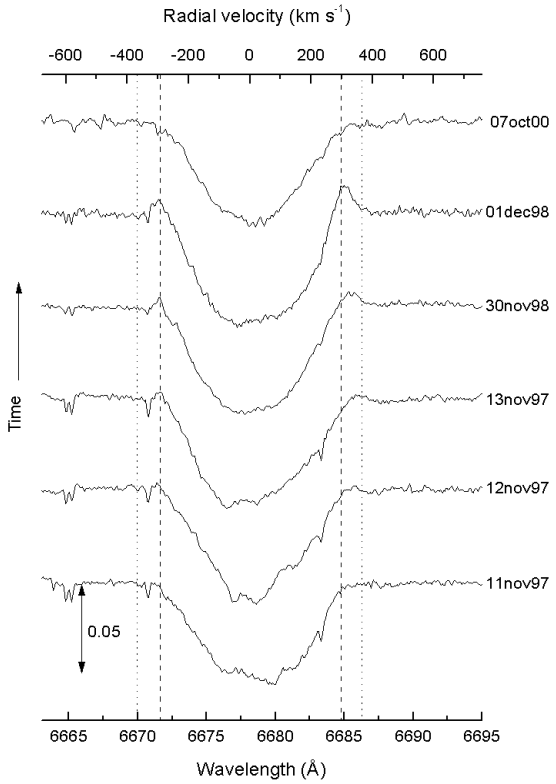

Fig. 9. Average line profiles of each night for the He I λ6678 Å from 1997 to 2000 epoch. The profiles are vertically displaced in time. Dates are indicated at right. The relative flux scale is indicated at the bottom left by the double arrow. The vertical dashed lines give the narrowest base width of the absorption profile ever present in our data sample [$\pm$294 km s^{-1}]. The vertical dotted lines displays the critical velocity limits.

approaches more closely the unperturbed photospheric line. In this line profile we see that the radial velocity limits may extend up to the stellar photosphere absorption $|RV| \simeq 294 \pm 1$ km s^{-1}, which is roughly 50 km s^{-1} wider than the expected projected true rotational velocity of the star $V \sin i = 242$ km s^{-1} and close to the projected critical rotational velocity $V_c \sin i = 286$ km s^{-1}. Since the stellar projected rotational velocity was derived from the He I4471 line, which is much less perturbed by circumstellar matter and because the same values are obtained at different epochs, it is unlikely that the star rotates at the critical velocity. Among the simplest explanations that may account for this phenomenon is that there is matter close to the star up to $R \sim 1.2 R_e$ that forms a pseudo-photosphere (Harmanec 2000), which is able to keep the line profiles apparently unperturbed and symmetrical. The emission shoulders, as well as some drifting bumps inside the line, can be explained in terms of orbiting clouds (Zorec et al. 2004). As we have no other approach to the genuine stellar He I λ6678 line profile, we used the 2000-year profile as a reference to represent the "quiet" photosphere and compared to it all individual He I λ6678 profiles to derive the λ-dependent standard deviations for the 1997 and 1998 observing period. The wavelength-dependent standard deviation gives an "image" of the way stellar and circumstellar activities affect different wavelengths inside the line profile. The λ-dependent standard deviations thus calculated for each observing epoch are shown in Fig. 10. We also used a reduced χ^2-test to estimate the significance level of deviations. It consists of obtaining the χ^2 from the λ-dependent profile deviations with respect to the average 2000-epoch reduced by the above λ-dependent variance. The standard tables of reduced χ^2

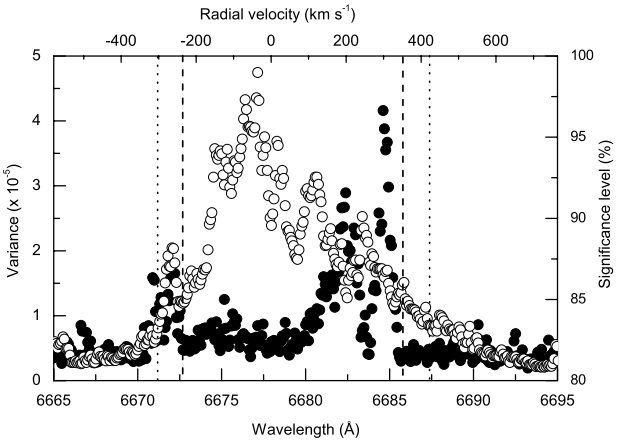

Fig. 10. Standard deviations against λ for 1997 (open circles) and 1998 (filled circles). The vertical dashed lines are the "empirical" photospheric radial velocity edges mentioned in the text [± 294 km s^{-1}], while the vertical dotted lines displays the critical velocity limits.

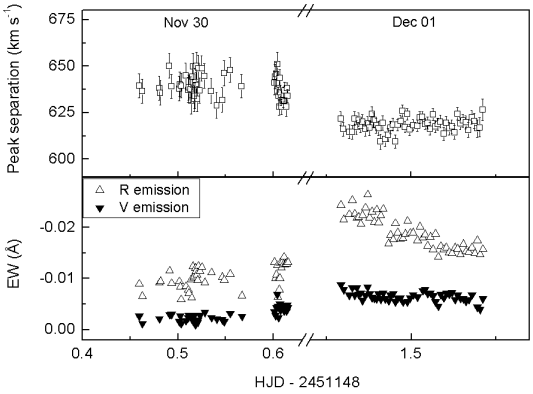

Fig. 11. *The upper panel* shows the peack separation behavior of blue and red emissions in the He I λ6678 Å line during the 1998 epoch against time. The error bars represent the standard mean absolute deviations. *The lower panel* shows the respective equivalent widths of blue and red emissions. The open triangles represent measurements of the red emission, while the filled triangles are for the blue emission. The nights are indicated on top of the first panel. The abscissa has a cut to omit the separation by one diurnal lapse of time between consecutive observations.

gives the significance level of deviations which are given in the right-side ordinate of Fig. 10.

The noteworthy observed changes are: 1) deviations are on average larger in 1997 than in 1998; 2) in 1997 they extend asymmetrically from about -400 to $+500$ km s^{-1}; 3) in 1998 they range roughly from -350 to $+350$ km s^{-1}; 4) there are two outstanding "activity maxima" in the 1998 deviation distribution around $RV \simeq \pm 300$ km s^{-1} of which the red one is the strongest. Strong global changes in the line profiles also occur from night to night. As shown in Fig. 9, in the 1997 epoch changes are seen mostly in the line core, while those in the 1998 epoch concern the line wings.

For comparison in Figs. 9 and 10 the radial velocity limits are drawn corresponding to the critical velocity of the the star.

4.4. Peak separation and equivalent widths

In the 1998 epoch, the He I λ6678 Å line profiles show emission shoulders in both blue and red wings (cf. Fig. 11) whose centroids are roughly at -300 and $+308$ km s^{-1}. Some Be stars may present He I line variations even during the photospheric CE quiescent phases (Rivinius et al. 1998). This variability concerns, in particular, the separation of emission peaks in the line wings and their intensity. Rivinius et al. (1998) pointed out that in μ Cen the separation of the emission peaks reaches its maximum during the precursor phase of outbursts. This separation then progressively diminishes in the relaxation phase of outbursts, during which the He I lines are the first to attain quiescence. We have measured the equivalent widths of the emission peaks in the He I λ6678 line and their separation in the 1998 epoch. The upper panel of Fig. 11 shows the behavior of the separation peaks, while the lower panel shows their equivalent widths. We can see that the separation changes from about 640 km s^{-1} to 620 km s^{-1} from one night to another and that this change occurs in few hours. Simultaneously, the equivalent width of the emission peaks in both wings increases, being four times larger in the red side than in the blue. After the increase of emission, which also operates over some hours, a slight and progressive decrease of the emission in both sides is noticed during the second night.

4.5. Line behavior and mass-ejection

In accordance with the behavior of the absolute deviation σ_λ presented in the preceding sections, the emissions that produce them could only have originated in some ejected matter that is orbiting the star. It was already noted by several authors (cf. Cidale & Ringuelet 1989; Hummel 1994; Chauville et al. 2001) that the separation of the emission peaks produced in the circumstellar media depends both on their kinematic characteristics and opacity. The intensity of the He I λ6678 line emission scales as $E \sim S_\lambda R^2(1 - \mathrm{e}^{-\tau_\lambda})$, where S_λ is the source function, R is a length scale (radius) of the emitting region and τ_λ is the optical depth in the line. The increase of the emission, mainly in the red wings, can then be understood as due to a rapid supply of matter by the star to the circumstellar environment, whose volume grows as it reaches the orbiting phase where positive radial velocities dominate. It was shown in Floquet et al. (2000) that the He I λ6678 line has a collisionally dominated source function and that near the star this source function remains constant as the emitting region expands. As the orbiting cloud expand/dissipate, their average radius R or scaling dimension increase. Not only must the emission intensity then increase, since $E \propto R^2$ and $S_\lambda \simeq$ const., but the opacity τ_λ decreases, because $\tau_\lambda \propto \int N_{\mathrm{HeI}} \mathrm{d}R$ and $N_{\mathrm{HeI}} \propto R^{-3}$. For low enough opacities the peak separation becomes dominated by the kinematics of the emitting layers. The growing value of R, which also implies the increase of the orbital radius and a consequent lowering of the tangential velocity component v_ϕ, reduces the separation of the emission peaks, as observed (see Fig. 11).

From the preceding sections we may conclude that during the phase of minimum Hα line emission intensity, the He I λ6678 line reveals circumstellar activity which persists

even through the Hα emissionless epoch. Although there is no direct indication of mass ejection phenomena, the emission in the extremes of the He I λ6678 line wings are signatures of circumstellar clouds.

5. Long-term Hα line variation and characteristics of the CE in α Eri

Apart from stellar activity detected through the lpv of photospheric lines, there are long-term variations of lines formed in the CE which bring information on the global physical evolution of the CE. The changes in the characteristics of the CE are probably not only due to one discrete mass ejection, but to the piling up phenomenon of matter coming from many discrete ejections, to the relentless interaction of more or less variable stellar winds with the ejecta (Hartquist et al. 1986; Dyson & Hartquist 1992; Arthur et al. 1994), to viscous redistribution of angular momentum (Porter 1999; Okazaki 2001; Clark et al. 2003) and to accelerations by magnetic fields (Balona 2002; Neiner et al. 2003). Then, correlations may not exist between the observed rapid variations of photospheric lines and the long term changes of lines raised in the CE. So, we investigate: 1) what are the orders of magnitude of parameters like the CE mass and the CE dimensions responsible for the observed Hα line emission and thus, is the CE, present at the moment of interferometric measurements, able to produce some IR radiation excess at λ2.2 μm that perturbed the photospheric one; 2) to which phase of long-term variation of the Hα emission do the short-term activity produced by mass around the star correspond; 3) what are the characteristics of the CE evolution in α Eri.

5.1. Characteristics of the Hα line emitting region from 1991 to 2002

The Hα line of α Eri was observed several times from 1991 to 2002. The Hα line profiles of 2002 were obtained halfway through the period of interferometric observations. Since the 1999 line profile seemed to have no emission, we used it to represent the stellar photospheric absorption profile and subtracted it from all remaining Hα lines observed. The Hα line emission components thus obtained are shown in Fig. 12, where we also added in the bottom of the figure the adopted photospehric absorption Hα line profile. We insist on the importance of the 1999 Hα line profile because it helped us to reveal the tiny emission components of 1998, 2000 and 2002 that otherwise would be difficult to see. The respective raw Hα line profile could easily be misinterpreted as of normal-like absorption nature.

In this section we evaluate the order of magnitude of physical parameters that characterize the CE regions responsible for each Hα line emission shown in Fig. 12. They will help us, on one hand, to determine whether the CE at the moment of interferometric observations could perturb the interferometric measurements. On the other hand, they may clarify the circumstellar disc formation/variation around α Eri.

According to the discussion in Sect. 3.5, the star is seen at an inclination $i \gtrsim 70°$. So, to simplify the formulations of the Hα line emission formation in α Eri we assume that the star-disc system is observed equator-on. The CE is taken as a disc with uniform half-height H, where the number density distribution of particles is described by the power law:

$$\frac{N(R)}{N(R_{\rm o})} = \left(\frac{R_{\rm o}}{R}\right)^{\beta}. \tag{9}$$

It can be shown that 95% of the emission in the Hα line is formed in a region delimited by an internal and an external radius: $R_{\rm o}$ and $R_{\rm E}$ respectively (Rohrmann 2000), whose values depend on β and $T_{\rm eff}$. To simplify the treatment of the Hα line emission formation, the emitting region can be reduced to an equivalent thin ring having the same particle column density and total mass as the "actual" contribution zone. Using the definition $H^{(n)}(x,\beta) = (x^{n-\beta})/(n-\beta)$ to shorten the notation that verifies $\lim_{\beta\to n} H^{(n)} = \ln x$, the radius of the ring $R_{\rm r}/R_{\rm o}$ is then given by:

$$\frac{R_{\rm r}}{R_{\rm o}} = \frac{H^{(2)}(R_{\rm E},\beta)}{H^{(1)}(R_{\rm E},\beta)}. \tag{10}$$

Since the ring also summarizes the entire rotational velocity field in the Hα line emitting zone, the rotational velocity of the ring $V^{\rm r}_{\Omega}$ is a function of the rotational velocity law and of the matter density distribution in the disc. Assuming that the rotational velocity law in the disc is $V_{\Omega}(R) \sim R^{-\gamma}$ and asking the equivalent ring preserves the azimuthal mass-flux, we obtain the following relation:

$$V^{\rm r}_{\Omega} = V^{\rm o}_{\Omega}\frac{H^{(1)}(R_{\rm E},\beta+\gamma)}{H^{(1)}(R_{\rm E},\beta)}. \tag{11}$$

Because we do not have enough physical constraints to infer the value of γ, we assume $\gamma = 0.5$ as if the disc were in Keplerian rotation. Some values of $R_{\rm r}/R_{\rm o}$ and $V^{\rm r}_{\Omega}/V^{\rm o}_{\Omega}$ for $\gamma = 0.5$ as a function of $R_{\rm E}/R_{\rm o}$ and β are given in Table 5. Relations (10) and (11) are useful to estimate the particle density distribution parameter β, once $R_{\rm r}/R_{\rm o}$ and $V^{\rm r}_{\Omega}$ are determined from the best fits of the observed Hα line emission profiles. The parameter β will enable us to calculate the IR continuum radiation produced by the CE near the star.

The source function $S_{\rm H\alpha}$ of the Hα line in CE surrounding B-type stars is dominated by radiative ionization and recombination processes of atomic levels (Thomas 1965; Jefferies 1968). Then, in the ring holds the following dependence of the source function with the optical depth (Mihalas 1978):

$$S_{\rm H\alpha}(\tau_{\rm o}) = \begin{cases} \eta^{1/2}B^* & \text{for } \tau_{\rm o} \le 1 \\ \eta^{1/2}B^*\tau_{\rm o}^{1/2} & \text{for } \tau_{\rm o} > 1, \end{cases} \tag{12}$$

where $\tau_{\rm o}$ is the optical depth in the central wavelength of the Hα line; η is the radiative "sink" term; B^* is the "source" factor of $S_{\rm H\alpha}$. At electron temperatures $T_{\rm e} \sim 0.8 \times T_{\rm eff}$ and electron densities $N_{\rm e} \lesssim 10^{13}$ cm^{-3} the expressions for the sink and the source factors η and B_* become respectively:

$$\left.\begin{aligned} \eta &\simeq R_{3k}/A_{32} \\ B^* &\simeq \tfrac{2h\nu^3_{\rm H\alpha}}{c^2}\left[{\rm e}^{h\nu_{\rm H\alpha}/kT_{\rm e}}\tfrac{R_{3k}}{R_{2k}}\tfrac{R_{k2}}{R_{k3}} - 1\right]^{-1} \end{aligned}\right\}, \tag{13}$$

where R_{nk} and R_{kn} are the radiative ionization and recombination rates to the n-atomic level respectively and A_{32} is the

Table 5. Ring radius R_r/R_o and V^r_Ω/V^o_Ω as a function of R_E/R_o and β.

β =	0.0	1.5	2.0	0.0	1.5	2.0
R_E/R_o		R_r/R_o			V^r_Ω/V^o_Ω	
2.0	1.5	1.4	1.4	0.83	0.85	0.86
5.0	3.0	2.3	2.0	0.62	0.72	0.76
10.0	5.5	3.2	2.6	0.48	0.66	0.72
15.0	8.0	3.9	2.9	0.41	0.63	0.70
30.0	15.5	5.5	3.5	0.31	0.59	0.69

Table 6. CE parameters from fits of Hα emission line profiles.

Epoch	τ_o	R_r/R_o	H/R_*	V^r_Ω	V_{rad}	β
				km s^{-1}		
1991	0.15	3.8	3.8	265	0	1.8
1993	1.18	6.0	3.5	197	0	0.2
1994	0.70	5.9	3.8	185	0	–0.1
1995	0.25	5.5	3.5	190	–10	0.1
1998	0.09	3.8	3.5	275	50	2.0
2000	0.08	3.8	2.2	220	255	–0.4
2002	0.13	3.7	2.5	270	–15	1.9

spontaneous emission rate. From Eq. (13) we see that the radiation field of the underlying star determines entirely the value of the source function, so that $\eta^{1/2}B^*/F_* = 0.08$, where F_* is the stellar continuum flux.

We assumed that in the CE the pressure broadening effects on the line can be neglected. The wavelength-dependent H α line optical depth is then written as:

$$\tau_\lambda = \tau_o \Phi(\Delta\lambda) \quad (14)$$

where Φ is the Gauss function. The wavelength displacement $\Delta\lambda$ is produced by the total velocity of the ring projected along the line of sight $\pm\mu V_{rad} \pm (1-\mu^2)^{1/2} V^r_\Omega$, where V_{rad} is the velocity in the radial direction; V^r_Ω is the ring rotational velocity; μ = cos (radial direction, line of sight); the signs are chosen according to the quadrant of the ring facing the observer and whether it concerns the front or rear part of the ring.

The observed Hα line profiles were fitted with the calculated ones using a least squares minimizing method, where R_r/R_o, $\overline{H/R_*}$, V_{rad}, V^r_Ω and τ_o are free parameters. In general V_{rad} accounts for the asymmetry seen in the emission peaks. The separation of the emission peaks is determined mainly by V_Ω, but it also depends on τ_o. The full width of the emission line at its half intensity is fixed by V^r_Ω, R_r/R_o and τ_o. For a given value of R_r/R_o, H/R_* and τ_o determine the emission intensity in the peaks and the depth of the central absorption.

The fits obtained are shown in Fig. 12 (dashed lines). The corresponding CE parameters are given in Table 6. We note that using the Gauss function to represent Φ we could not obtain a good fit of the Hα line emission wings in 1993. The wide wings could be due perhaps, among others, to changes in the average photospheric Hα line profile produced by the stellar surface activities. In our approach these changes were overlooked, because we used the same absorption photospheric line profile for all observed epochs.

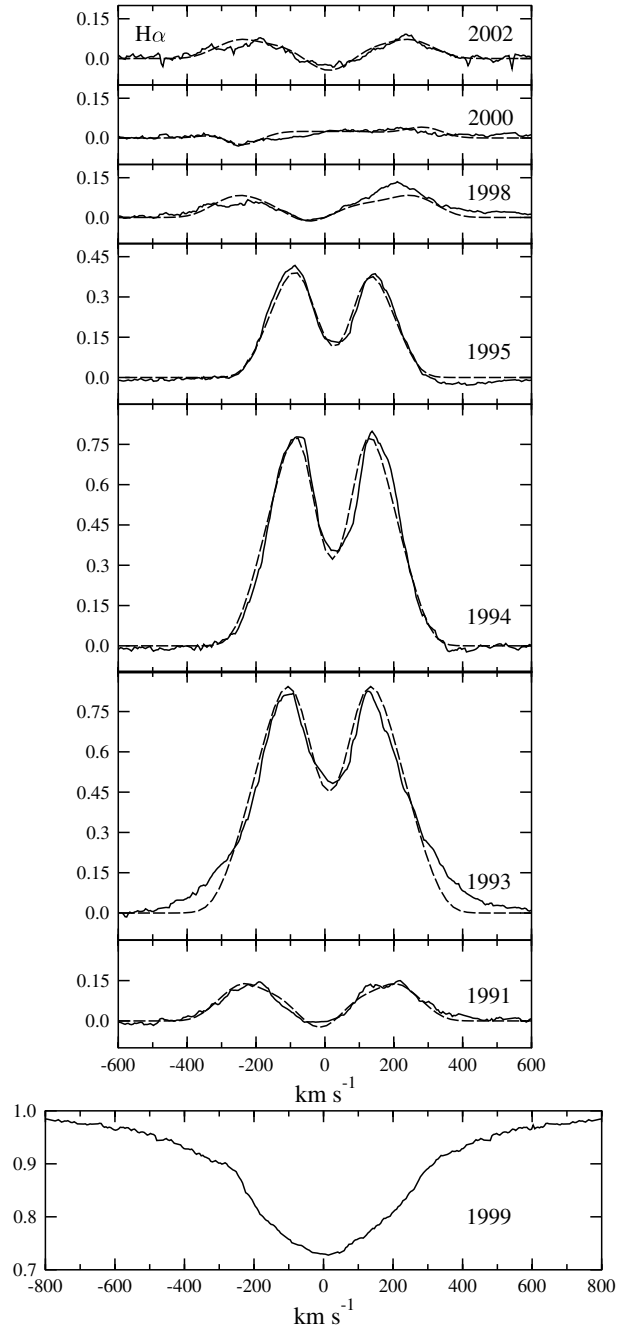

Fig. 12. Hα line profiles from 1991 (*bottom*) to 2002 (*top*). These profiles have the photospheric line component subtracted, so that the continuum level is set to zero. Observed profiles are in full lines and model fits are in dashed lines. In the bottom the Hα line profile in 1999 is shown that we considered to represent the photospheric absorption.

5.2. Characteristics and evolution of the circumstellar disc

In general, a non negligible ring/disc effective height $H/R_* \sim 3.4 \pm 0.6$ is required. This is the consequence of the small source function determined only by the stellar effective temperature

due to its radiative nature, which implies that in the case of a disc seen equator-on, the projected emitting surface towards the observer must be large enough to recover enough Hα line emission. Within the model simplifying characteristics, the flattening of the disc shaped CE is $H/R_{\rm E}$, where $R_{\rm E} \gg R_{\rm r}$.

Over the whole 1991–2002 period we distinguish three types of Hα line emission profiles which are characterized by as many different structures of the CE. The line profiles in 1991, 1998 and 2002 are of rather the same class. The corresponding estimated values of β imply on average quite extended emitting regions $\langle R_{\rm E}/R_{\rm o}\rangle \simeq 40$ with outward rather steeply decreasing density distributions: $\beta \sim 2$.

Another type of Hα line profile is displayed in the period from 1993 to 1995. In this time interval the CE is marked by a quite stable value of the emitting region extent $\langle R_{\rm E}/R_{\rm o}\rangle \simeq 11 \pm 3$ with nearly the same disc height $\langle H/R_*\rangle \simeq 3.6 \pm 0.1$ and a quite uniform density distribution: $\beta \sim 0$. However, during this period the amount of mass gathered in the emitting zone changed somewhat, because the line opacity $\tau_{\rm o}$ progressively decreased from ~1.2 in 1993 to ~0.3 in 1995. A nearly uniform particle density distribution ($\beta \sim 0.0$) seems to be a condition for a CE high emitting effectiveness in the Hα line.

The overall decrease of $\tau_{\rm o}$ from 1993 to 1998 could be due to an emptying phenomenon of the mass content in the disc, accompanied by a stretching of the CE emitting region. This might explain the region how could attain in 1998 a steep density distribution ($\beta \sim 2$). We notice that almost the same CE structure must have existed in 1991, just before the Hα line emission started rising towards its maximum.

The fitting parameters given in Table 6 indicate that while almost all profiles require no velocity in the radial direction of the CE, there must be a rather strong expansion in the 2000 epoch. The faint emission seen in this epoch, which has an incipient P Cygni component, requires a rapid expansion velocity in the bulk of the Hα formation region, although decelerating outwards to account for $\beta \lesssim 0.0$ which also implies a piling up phenomenon of mass far from the star.

5.3. The circumstellar matter at the epoch of interferometric measurements

To obtain insight into the amount of matter around the star at the epoch of interferometric observations and see whether it could produce some IR flux excess, we assume, as we did for the Hα line interpretation, that the particle number density distribution in the CE is described by Eq. (9). We also take the radial dependence of the temperature in the disc, $T_{\rm e}(R)$, determined by the geometrical dilution of the stellar bolometric radiation field (Moujtahid et al. 2000a,b). The disc is made of hydrogen and a fraction $N({\rm He})/N({\rm H}) = 0.1$ of helium. All calculations are performed under LTE conditions. It can be shown then that for $T_{\rm eff} = 15\,000$ K the electron density distribution $N_{\rm e}/N_{\rm e}^*$ in the CE up to some $R_{\rm b}$ depends both on β and the temperature $T_{\rm e}(R)$ ($N_{\rm e}^*$ is the electron density at $R = R_*$). Beyond a distance $R_{\rm b}$ the ratio $N_{\rm e}(R)/N_{\rm e}(R_{\rm b})$ is determined almost entirely by $T_{\rm e}(R)$. Electron density distributions $N_{\rm e}^*(R)$ are shown in Fig. 13 for $T_{\rm eff} = 15\,000$ K, $N_{\rm e}^* = 10^9$ and 10^{12} cm^{-3} and different values of β.

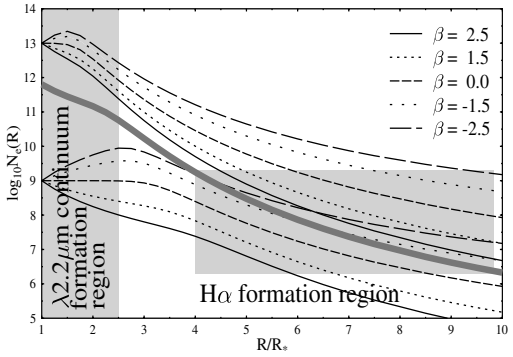

Fig. 13. Electron density in the disc as a function of the distance from the star for different particle distribution laws $N \sim R^{-\beta}$ and electron densities $N_{\rm e}^*$ near the star. The shaded zones represent schematically the IR $\lambda 2.2$ μm continuum excess and Hα line emission formation regions in the disc during the 2002 epoch. The thick curve represents the electron density distribution in the CE deduced for the 2002 epoch.

Since the absorption cross-section in the center of the Hα line is by factors larger than the total continuum absorption cross-section due to Thomson scattering, free-free and hydrogen bound-free transitions at $\lambda \sim 2.2$ μm, the disc regions contributing to the IR radiation at $\lambda \sim 2.2$ μm must be closer to the central star than those implied by the Hα line emission. To estimate the electron densities in both Hα line emission formation region and in the continuum $\lambda 2.2$ μm emitting zone we looked first for densities that reproduce the opacity $\tau_{\rm o} = 0.13$ corresponding to the Hα line emission in 2002. This was done by integrating the specific intensity in the center of the line outside-in in the radial direction over a disc extent that contribute to the total emission from 10 to 95% in the line center. The specific intensity in the center of the line and in the radial direction is given by:

$$I = \int_0^{\tau_{\rm o}} S_{\rm H\alpha}(R) {\rm e}^{-\tau(R)} {\rm d}\tau(R) \qquad (15)$$

where $S_{\rm H\alpha}$ is the source function defined by Eqs. (12) and (13) and $\tau(R)$ is the outside-in optical depth of the disc in the central wavelength of Hα. The so-called "formation region" depends then on $\tau_{\rm o}$, β and $N_{\rm e}^*$. The 2002 Hα line emission formation region in the disc is shown in Fig. 13 by the horizontal shaded bar. Given the values $\tau_{\rm o} = 0.13$ and $\beta = 1.9$ we could estimate $N_{\rm e}^* = 6.3 \times 10^{11}$ for the 2002 epoch.

The most important consequence of this calculation is that it enables us to estimate the amount of energy emitted by the circumstellar disc in the IR continuum at $\lambda_{\rm eff} = 2.175$ μm near the star in the 2002 epoch of interferometric measurements. To this end we used a similar expression to Eq. (15) for the continuum radiation specific intensity, but for a source function and opacity due to electron scattering and (bound-free)+(free-free) hydrogen transitions. We calculated a grid of specific intensities $I(x, y)$, where (x, y) are Cartesian coordinates in the plane of the sky with the x-axis parallel to the stellar equator. We assumed the central star limb and gravitationally darkened. Figure 14 shows the specific intensity emerging from the

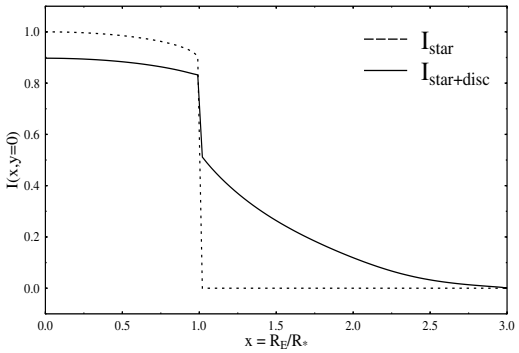

Fig. 14. Specific intensity $I(x, y = 0)$ (full line) at the equator emitted by the star+disc system compared to the specific intensity $I_*(x, y = 0)$ (dotted line) at the equator emitted by the star alone.

star+disc system (full line) corresponding to the equatorial region ($y = 0$). In the figure is also shown the specific intensity of the star without CE. In the polar direction ($x = 0$), the specific intensity map is given simply by the "absorbed" stellar-like component seen in Fig. 14, without the intensity tail at $R > R_*$. We readily note that the effective continuum emitting region in the equator does not extends further than some 2.5 R_*. The disc, although it emits, produces an emerging radiation that looks like absorbed stellar radiation, which reduces the contrast to the adjoining emitted radiation by the disc outside the stellar disc. The resulting flux in $\lambda_{\rm eff} = 2.2$ μm from the star+disc system, calculated from the entire grid of calculated intensities $I(x, y)$ and for a disc of uniform height $H = R_*$, is just $(F - F_*)/F_* = 0.27$. However, in spite of this low flux excess, there is a high contrast between the equatorial and the polar map of the emitted continuum radiation intensities, which can mimic an apparently enlarged stellar equatorial extent. It was shown by Domiciano et al. (2002) that the interferometric complex visibility amplitude is a sensitive function of the shape and the surface intensity map of the emitting source. Moreover, Tycner (2004) has also derived a correction to the argument of the visibility amplitude needed when the light source is reduced to an equivalent uniform elliptical source and included corrections to the complex visibility carried by the circumstellar radiation.

The modeling of the visibility amplitudes for stars with CE is out of the scope of the present paper. The detailed interpretation of the interferometric observation of α Eri should enable us, however, to draw information on the disc structure in the perpendicular direction to the equator, since the intensity map and the corresponding complex visibility depend strongly on it.

6. Discussion

6.1. Other geometries of circumstellar discs

The constant-height model used in the preceding sections is only one possible geometrical disc configuration among many others. From physical first principles and the kinetic theory of gases applied to steady-state self-gravitating gaseous masses with cylindrical differential rotation, circumstellar discs should have isodensity surfaces with lemniscate-like vertical cuts (Schmitz 1983; Rohrmann 1997). However, in current Be star disc modeling authors frequently use spreading out circumstellar structures. We adopt the model proposed by Waters (1986) as representative of flaring up discs and inquire whether and how our previous conclusions on disc structures need to be reinterpreted in terms of these other circumstellar structures.

Table 7. Ring radius $R_{\rm r}/R_{\rm o}$ and $V^{\rm r}_\Omega/V^{\rm o}_\Omega$ as a function of $R_{\rm E}/R_{\rm o}$ and β for flaring discs.

$\beta =$	0.0	1.5	2.0	0.0	1.5	2.0
$R_{\rm E}/R_{\rm o}$		$R_{\rm r}/R_{\rm o}$			$V^{\rm r}_\Omega/V^{\rm o}_\Omega$	
2.0	1.6	1.6	1.5	0.81	0.84	0.85
5.0	3.7	3.0	2.7	0.57	0.65	0.69
10.0	7.3	5.3	4.4	0.41	0.53	0.59
15.0	10.9	7.5	5.9	0.34	0.47	0.55
30.0	21.7	13.9	9.8	0.24	0.38	0.48

Again, we take a radial distribution of particle densities given by Eq. (9), where β masks all intervening factors that redistribute the matter around the star in a flaring up disc. The line emission produced by such a disc, as seen by an equator-on observer, can also be sketched with an equivalent emitting surface as we attempted in the preceding sections. However, the surface density of particles in an equivalent cylinder perpendicular to the equator is now a function of the vertical coordinate z:

$$\sigma(z) = N_{\rm o} R_{\rm o} [H^{(1)}(R_{\rm E}, \beta) - h(z)/(1 - \beta)] \tag{16}$$

where $h(z) = 1$ for $z \leq R_{\rm o} \tan\phi$ and $h(z) = (z/R_{\rm o} \tan\phi)^{1-\beta}$ for $z > R_{\rm o} \tan\phi$; ϕ is the semi-opening angle of the disc. Since $\sigma(z)$ scales the particle column density as a function of z, the emission efficiency is also a function of z, contrarily to our previous model where it is constant with z. Due to the competing emission and self-absorption effects according to z, carried by the z-dependent opacities, only more or less detailed calculations of the emission in lines that are out of the scope of this discussion could allow us to determine as a function of specific disc parameters whether the contribution to the global emission is stronger from regions $z \to 0$ or from higher z. This may, however, have consequences for the estimation of the average optical depth and radius $R_{\rm r}$ of the equivalent emitting surface. The relation for flaring discs that replaces Eq. (10) is now:

$$\frac{R_{\rm r}}{R_{\rm o}} = \frac{(\beta - 1) H^{(3)}(R_{\rm E}, \beta)}{H^{(2)}(R_{\rm r}, \beta) + 1 - (R_{\rm E}/R_{\rm o})^{1-\beta} (R_{\rm r}/R_{\rm o})}. \tag{17}$$

In the same way, the relation equivalent to Eq. (11) becomes:

$$V^{\rm r}_\Omega = V^{\rm o}_\Omega \frac{H^{(2)}(R_{\rm E}, \beta)}{H^{(2)}(R_{\rm E}, \beta + \gamma)}. \tag{18}$$

Table 7 gives estimates of $R_{\rm r}/R_{\rm o}$ drawn from Eq. (17) and $V^{\rm r}_\Omega/V^{\rm o}_\Omega$ ratios for the same $R_{\rm E}/R_{\rm o}$ and β parameters as in Table 5.

As noted above, in flaring discs the line emission production has specific characteristics which can lead to fitting radii $R_{\rm r}$ slightly different to those inferred from the constant-height discs. Relations (17) and (18) weigh disc properties at

slightly larger radii than Eqs. (10) and (11). However, the ratios $V^{\rm r}_{\Omega}/V_{\Omega}(R_{\rm r})$ are the same in both cases. On the other hand, we do not expect the flaring discs to produce much larger effective radii $R_{\rm r}$, because the consequently lower local average temperature increases the hydrogen recombinations ($\mathcal{R} \propto T_{\rm e}^{-1/2}$) and the larger emitting surface can rapidly produce too high a line emission. It is expected that the β parameters inferred using flaring out discs may not differ strongly from those derived with constant-height discs.

In the flaring up discs the particle surface density has specific behavior according to the value of β. From Eq. (16) the average surface density as a function of the radius R is:

$$\frac{\overline{\sigma(R)}}{N_{\rm o}R_{\rm o}} = H^{(1)}(R_{\rm E},\beta) + \frac{1+[1+(R_{\rm o}/R)]H^{(2)}(R,\beta)}{1-\beta} \qquad (19)$$

which for β values similar to those found from emission line fitting with constant-height disc models become:

$$\frac{\overline{\sigma(R)}}{N_{\rm o}R_{\rm o}} = \begin{cases} R_{\rm E}/R_{\rm o} - R/R_{\rm o} & \beta = 0 \\ \ln R_{\rm E}/R_{\rm o} & \beta = 1 \\ (\ln R/R_{\rm o}+1)(R_{\rm o}/R) - R_{\rm o}/R_{\rm E} & \beta = 2. \end{cases} \qquad (20)$$

Thus, $\beta \simeq 0$ implies a linear decrease of the average surface density, for $\beta \simeq 1$ it is $\overline{\sigma(R)}$ = constant and for $\beta \simeq 2$ it would decrease with R very slowly.

These examples show that as long as we do not know the precise geometry of Be star discs, even the simplest attempts to avoid "qualitative" interpretations of disc shapes and their behavior, cannot avoid conclusions that are still somewhat model-dependent.

6.2. Cyclic long-term Hα line emission changes

The description of the Hα line emission profiles carried out in Sect. 5.2 concerns an entire cycle of B→Be→B phase transition. We take advantage of these observations to obtain information on the time scales of Hα emission changes, by comparing them with previous long-term Hα variations in α Eri. The time scales of these cycles are important to understand the disc formation mechanisms (Porter 1999; Okazaki 2001).

We collected in the literature the spectroscopic and photometric records of the Hα line variation and studied them as a function of time. The data used are from Jaschek et al. (1964), Andrews & Breger (1966), Dachs et al. (1977, 1981, 1986, 1992), Slettebak (1982), Freitas-Pacheco (1982), Balona et al. (1987), Porri & Stalio (1988), Hanuschik et al. (1996). The photometric measurements of the Hα line given in some of the above papers were transformed into equivalent widths.

The definition of the equivalent width for the Hα line emission component used in this paper is:

$$W_{\rm H\alpha} = \int_{-\infty}^{\infty} \left(\frac{f_\lambda - f^*_\lambda}{f^*_{\rm c}} \right) \quad (\text{Å}) \qquad (21)$$

where f_λ is flux in the line emission component, f^*_λ is the flux in photospheric absorption component and $f^*_{\rm c}$ is the flux of the stellar proper adjacent continuum flux, which was assumed unchanged by the CE emission/absorption. From Eq. (21) it follows that to a B-normal like phase corresponds $W_{\rm H\alpha} = 0$, while for an emission phase we have $W_{\rm H\alpha} > 0$.

The variation of the equivalent width of the Hα line emission component before 1991 is shown in Fig. 15a. In this figure we also added the qualitative estimates of the emission intensity noted in the literature before 1965. The changes of the Hα emission observed from 1991 to 2002 is shown in Fig. 15b. From both panels in Fig. 15 we conclude that there is a cyclic variation of the Hα line emission. The maxima of emission are attained roughly every 14 years, while the onsets of the increase towards the greatest emission maxima occur every 15 years. Figure 15 shows that the two last B-normal like aspects lasted 4 to 5 years. From the last two cycles we learn that after the quiescent, or B-normal like phases, the star resumes its maximum emission in no more than 2 years. We can also see that after each emission maximum there is a 4–5 year plateau of weak emission before the star recovers the B-normal appearance. These time scales may have some significance in modelling the CE formation in this star.

The activity detected in the He I λ6678 line, mainly the one in 1998 that we interpreted as from a possible mass ejection, happened during a phase of the Hα emission decline. Unfortunately, no information on the stellar activity and/or possible mass ejection can be obtained from the records we have of the He I λ6678 line in 1999, because the spectra cannot be exploited.

If the evolution of the CE in α Eri, i.e. formation and subsequent dissipation, has to be understood in terms of a viscous decretion disc model (Porter 1999; Okazaki 2001), from the expected average viscous time scales for $t \sim 60/\alpha$ days (Clark et al. 2003), we would derive two quite different series of values for the viscosity coefficient α. The time scales implied by the CE formation, estimated from the time that the emission rise takes in the Hα line: about 2 years, we would obtain $\alpha \sim 0.08$, which is of the same order as expected for CE envelopes studied by Blondin & Negueruela (2001), Matsumo (1999) and Clark et al. (2003). The time required by the decrease from maximum to zero is either 10 years in the 1974–1989 cycle or 6 years during the 1991–2000 cycle. This implies $0.02 \lesssim \alpha \lesssim 0.03$, which is about 4 times smaller than that implied in the formation process. We may then wonder whether the bulk redistribution of material in the circumstellar disc occurs only as a consequence of a viscous redistribution of angular momentum.

7. Conclusions

Since rotation seems to be a key factor to initiate the Be phenomenon and because direct interferometric determinations of the shape of the brightest Be star in the sky produced a flattening that the present theories of fast rotating massive stars cannot account for correctly, in the present paper we explored an explanation of this unexpected result based on radiation fluxes emitted by possible circumstellar matter adjoining the central star. In 2002 the signatures of this matter almost entirely escaped spectroscopic detection in the visible spectral region.

We determined the stellar flattening looking for better correspondence of spectroscopic, spectrophotometric and interferometric measurements to the predictions of stellar atmosphere and evolution models of fast rotating stars. We inferred that

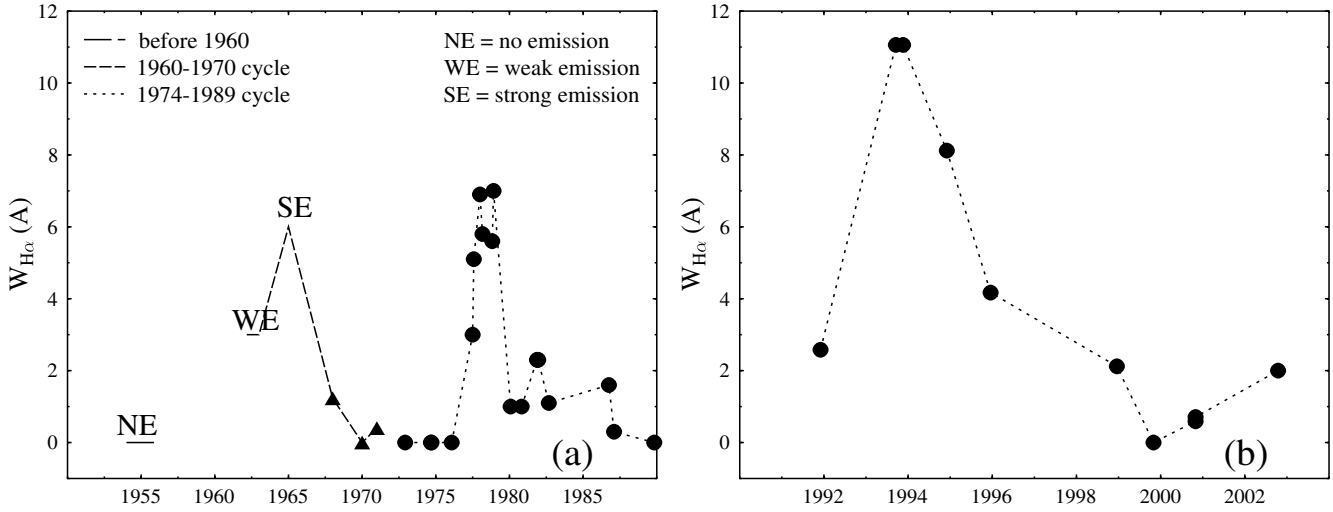

Fig. 15. Long-term variation of the equivalent width W in Å of the Hα line emission. **a)** Qualitative estimations of the emission strength (NE = no emission; WE = weak emission; SE = strong emission) and quantitative equivalent widths before 1990 collected in the literature. **b)** New equivalent widths obtained in this work after 1990. The equivalent widths used in both panels were determined using relation (21). Different markers were used to identify better the emission cycles that on average last 11 years.

α Eri rotates, at most, with an angular rotation rate $\Omega/\Omega_c \simeq 0.8$ which is less than the average rate found by Frémat et al. (2005) for the Galactic field Be stars. Due to the slightly over-critical flattening of the star deduced from the interferometric observations, we searched for possible explanations of this result in terms of flux excesses produced by an apparently elusive circumstellar matter.

We studied the short-term activities of α Eri. We performed time series analysis of variations detected in the He I and Mg II spectral lines with the CLEANEST algorithm. We used high S/N spectroscopic observations carried out from Nov. 1991 to Oct. 2000. Of particular importance are the observation made in Oct. 2000, because they are close to the most marked B-normal like phase of α Eri. Unfortunately, observations made in Oct. 1999 during the B-normal like phase of the star are unexploitable for *nrp* studies in the He I 6678 region. This analysis, carried on the He I 6678, He I 4922, He I 4471 and He I 4388 and Mg II 4481 lines, produced the following frequencies: $\nu = 0.49$, 0.76, 1.27 and 1.72 c/d. The frequencies 2.32 and 3.30 c/d are possible aliases of $\nu = 1.27$ c/d. We also estimated the following pulsation degrees: $\ell \sim 3$–4 for $\nu = 0.7$ c/d, $\ell \sim 2$–3 for $\nu = 1.27$ c/d and $\ell \sim 3$–4 for $\nu = 1.72$ c/d. Since we concluded that the rotational frequency of the star is $\nu_r = 0.57$ c/d, the lowest frequency ($\nu = 0.49$ c/d) can be produced by the circumstellar matter adjoining the star, while the remaining frequencies can be due to *nrp* of the central star. In general, the Mg II 4481 and He I 6678 are believed to carry information also on the activity in the CE near the central star. In Mg II 4481 only one outstanding frequency was detected: $\nu = 0.49$ c/d, which was present also in 1999 during the B-normal like phase. The $\nu = 0.49$ c/d is present also in the He I 6678 line profiles, but with different degrees of statistical significance. The ratio $\nu_r/\nu \simeq 1.2$ may then imply the existence of clouds at $R/R_* \sim 1.1$. These clouds can result from discrete mass ejections, but we cannot assert they are related to the non-radial pulsations described in this paper. We conclude from this that even during the phase in which the star approaches the most to a B-nomal like aspect, there are spectroscopic signatures for some matter surrounding the star.

We also studied the average absolute deviations of the He I 6678 line profiles with respect to the unperturbed photospheric line occurred in 1997, 1998 and 2000 observing epochs. We found that the stronger absolute deviations in 1997 are confined within a maximum asymmetric radial velocity interval $-400 \lesssim RV \lesssim 500$ km s^{-1} and within $|RV| \lesssim 350$ km s^{-1} in 1998, though the empirical photospheric line profile seems not to extend further out than $|RV| \lesssim 294 \pm 1$ km s^{-1}. According to the results shown by Zorec et al. (2004), the line behavior of He I 6678 shown in Fig. 9 can easily be explained in terms of elongated clouds orbiting near the star. This is consistent with the presence of the $\nu = 0.49$ c/d frequency. Unfortunately, the timing of our observations does not cover the entire circulation cycle of these clouds. This explains that their presence is revealed only by the emission on the red side of the line profiles. Depending on the length of clouds, they can, however, be present alternatively in both sides of the line profiles. We may then conclude that the absolute deviations shown in Fig. 10 may represent the sum of photospheric oscillations and of light fluctuations produced by orbiting clouds.

We studied the long-term variation of the Hα line emission in α Eri. We used a disc model to interpret the Hα line emission profiles observed from 1991 to 2002. We have provided a phenomenological description of these line profiles in terms of physical quantities that characterize their formation region in the CE. Since the observed Hα line profiles cover an entire cycle of a B$\rightleftharpoons$Be phase transition, we have concluded that: a) the low Hα emission phases are characterized by extended emission zones in the circumstellar disc with a rather steep outward matter density decline; b) during the strong Hα emission phases the emitting regions are less extended and have a rather constant density distribution.

The Hα line emission profile observed in 2002 at the epoch of interferometric measurements implies that there was enough matter adjoining the central star to produce an IR $\lambda 2.2$ μm radiation flux excess to mimic an enlarged stellar equatorial radius. Due to the α Eri effective temperature, excitation conditions of the circumstellar matter near the star are optimal to produce enough IR flux excess to perturb the measurements, while no detectable changes are produced in the visible energy distribution.

To complete the description of the long-term Hα line emission variation in α Eri, we noticed that the star has a long-term, roughly cyclical B$\rightleftharpoons$Be phase transition every 14–15 years. The disc formation time scales, interpreted as the periods during which the Hα line emission increases from zero to its maximum, agree with the viscous decretion model. On the other hand, the time required for the disc dissipation that ranges from 6 to 12 years is not consistent with the viscous disc model.

Acknowledgements. M.V.M.F. expresses his thanks to Dr. A. M. Hubert and M. Floquet for fruitful discussions. J.Z. warmly thanks Drs. Y. Frémat, A. Domiciano de Souza and F. Vakili. We are greatful to the anonymous referee for the comments and suggested corrections. This research was supported by Fundação de Amparo à Pesquisa do Estado de São Paulo through grants no. 99/12436-9 and 02/00036-0.

References

Alonso, A., Arribas, S., & Martínez-Roger, C. 1994, A&A, 282, 684
Ando, H. 1991, in Rapid Variability of OB-stars: Nature and diagnostics Value, ed. D. Baade, Garching, ESO, Eso Conf. Workshop Proc., 36, 303
Andrews, P. J., & Breger, M. 1966, Observatory, 86, 108
Arthur, S. J., Dyson, J. E., & Hartquist, T. W. 1994, MNRAS, 269, 1117
Baillet, A., Chalonge, D., & Divan, L. 1973, Nouv. Rev. Opt., 4, 151
Balona, L. A. 2000, in The Be Phenomenon in Early Type Stars, ed. M. A. Smith, H. F. Henrichs, & J. Fabregat, ASP Conf. Ser., 214, IAU Colloq., 175, 1
Balona, L. A., Engelbrecht, C. A., & Marang, F. 1987, MNRAS, 227, 123
Blondin, J. M., & Negueruela, I. 2001, A&A, 377, 161
Chalonge, D., & Divan, L. 1952, Ann. Astrophys., 15, 201
Chalonge, D., & Divan, L. 1973, A&A, 23, 69
Chauville, J., Zorec, J., Ballereau, D., et al. 2001, A&A, 378, 861C
Cidale, L. S., & Ringuelet, A. E. 1989, PASP, 101, 417
Cidale, L. S., Zorec, J., & Tringaniello, L. 2001, A&A, 368, 160
Clark, J. C., Tarasov, A. E., & Panko, E. A. 2003, A&A, 403, 239
Collins, G. W. 1973, A&A, 26, 315
Collins, G. W., & Truax, R. 1995, ApJ, 439, 860
Coté, J., & Waters, L. B. F. M. 1987, ApJ, 176, 93
Dachs, J., Maitzen, H. M., Moffat, A. F. J., Sherwood, W. A., & Stift, M. 1977, A&A, 56, 417
Dachs, J., Eichendorf, W., Schleicher, H., et al. 1981, A&AS, 43, 427
Dachs, J., Poetzel, & Kaiser, D. 1989, A&AS, 78, 487
Dachs, J., Hanuschik, R., Kaiser, D., Ballereau, D., & Bouchet, P. 1986, A&AS, 63, 87
Dachs, J., Hummel, W., & Hanuschik, R. W. 1992, A&AS, 95, 437
Divan, L., & Zorec, J. 1982, in The scientific aspects of the Hipparcos space astrometry mission, ESA-SP 177, 101
Domiciano de Souza, A., Kervella, P., Jankov, S., et al. 2003, A&A, 408, L47
Domiciano de Souza, A., Vakili, F., Jankov, S., Janot-Pacheko, E., & Abe, L. 2002, A&A, 393, 345
Dyson, J. E., & Hartquist, T. W. 1992, Astro. Lett. Comm., 28, 301
Emílio, M., & MSc Thesis 1997, IAGUSP
Floquet, M., Hubert, A. M., & Hirata, R., et al. 2000, A&A, 362, 1020
Foster, G. 1995, AJ, 109, 1889
Freitas-Pacheco, J. A. 1982, MNRAS, 199, 591
Frémat, Y., Zorec, J., Hubert, A. M., & Floquet, M. 2005, A&A, 440, 305
Gies, D. R., McKibben, W. P., Kelton, P. W., Opal, C. B., & Sawyer, S. 1990, AJ, 100, 1601
Gray, D. F. 1992, British Astron. Assoc. JNL, 102(4), 230
Guinan, E. F., & Hayes, D. P. 1984, ApJ, 287, L39
Hanbury Brown, R., Davis, J., & Allen, L. R. 1974, MNRAS, 167, 121
Hanuschik, R. W. 1995, A&A, 295, 423
Hanuschik, R. W., Dachs, J., Baudzuz, M., & Thimm, G. 1993, A&A, 274, 356
Hanuschik, R. W., Hummel, W., Dietle, O., & Sutorius, E. 1995, A&A, 300, 163
Hanuschik, R. W., Hummel, W., Sutorius, F., Dietle, O., & Thimm, G. 1996, A&AS, 116, 309
Harmanec, P. 2000, in The Be Phenomenon in Early Type Stars, ed. M. A. Smith, H. F. Henrichs, & J. Fabregat, ASP Conf. Ser., 214, IAU Colloq., 175, 13
Hartquist, T. W., Dyson, J. E., Pettini, M., & Smith, L. J. 1986, MNRAS, 221, 715
Henize, K. G., Wray, J. D., Parsons, S. B., et al. 1975, NASA-RP, 1031
Hiltner, W. A., Garrison, R. F., & Schild, R. E. 1969, ApJ, 157, 313
Hubeny, I. 1990, in Properties of hot luminous stars, Proceedings of the First Boulder-Munich Workshop, Boulder, CO, San Francisco, CA, ASP, 93
Hubeny, I. 1994, A&AS, 184, 3401
Hubert, A. M., & Floquet, M. 1998, A&A, 335, 565
Hubert, A. M., Floquet, M., & Zorec, J. 2000, in The Be Phenomenon in Early Type Stars, ed. M. A. Smith, H. F. Henrichs, & J. Fabregat, ASP Conf. Ser., 214, IAU Colloq., 175, 348
Hummel, W. 1994, A&A, 289, 458
Hummel, W., & Vrancken, M. 2000, A&A, 359, 1075
Jackson, S., MacGregor, K. B., & Skumanich, A. 2004, ApJ, 606, 1196
Jamar, C., Macau-Hercot, D., Monfils, A., et al. 1976, ESA SR-27
Jaschek, C., Jaschek, M., & Kucewicz, B. 1964, Z. Astroph., 59, 108
Jaschek, M., Slettebak, A., & Jaschek, C. 1981, Be Stars Newsletter, 4, 9
Jefferies, J. T. 1968, Spectral Line Formation (Massachusetts: Blaisdell Publishing Company)
Johnson, H. L., & Mitchell, R. I. 1975, Rev. Mex. Astron. Astrofis, 1, 299
Kaiser, D. 1987, A&AS, 67, 203
Kambe, E., Ando, H., Hirata, R., et al. 1993, PASP, 105, 1222
Keller, S. C., Bessell, M. S., Cook, K. H, Geha, M., & Syphers, D. 2002, AJ, 124, 2039
Kogure, T., & Hirata, R. 1982, Bull. Astr. Soc. India, 10, 281
Kurucz, R. 1994, Kurucz CD-ROM No. 19, 20, 21, Cambridge Mass.: Smithsonian Astrophysical Observatory
Leister, N. V., Janot-Pacheco, E., Leyton, J. Z., Hubert, A. M., & Floquet, M. 2000, in The Be Phenomenon in Early Type Stars, ed. M. A. Smith, H. F. Henrichs, & J. Fabregat, ASP Conf. Ser., 214, IAU Colloq., 175, 273
Levenhagen, R. S., Leister, N. V., & Zorec, J., et al. 2003, A&A, 400, 599
Mihalas, D. 1978, Stellar Atmospheres (San Francisco: W.H. Freeman & Co.)

Maeder, A., & Peytremann, E. 1970, A&A, 7, 120
Marlborough, J. M. 1976, in Be and shell stars, Proc. of the Merril-McLaughlin Memorial, ed. A. Slettebak, IAU Symp., 70, 335
Matsumoto, R. 1999, in Disk Instabilities in Cose Binary Systems, ed. S. Mineshige, & J. C. Weeler (Tokyo: Universal Academy Press.), 303
Mennickent, R. E., Pietrzyński, G., Gieren, W., & Szewczyk, O. 2002, A&A, 393, 887
Meynet, J., & Maeder, A. 2000, A&A, 361, 101
Moujtahid, A., Zorec, J., & Hubert, A. M. 1999, A&A, 349, 151
Moujtahid, A., Zorec, J., Hubert, A. M., Garcia, A., & Burki, G. 1998, A&AS, 129, 289
Moujtahid, A., Zorec, J., & Hubert, A. M. 2000a, in The Be Phenomenon in Early Type Stars, ed. M. A. Smith, H. F. Henrichs, & J. Fabregat, ASP Conf. Ser., 214, IAU Colloq., 175, 506
Moujtahid, A., Zorec, J., & Hubert, A. M. 2000b, in The Be Phenomenon in Early Type Stars, ed. M. A. Smith, H. F. Henrichs, & J. Fabregat, ASP Conf. Ser., 214, IAU Colloq., 175, 510
Neiner, C., Hubert, A. M., Frémat, Y., et al. 2003, A&A, 409, 275
Okazaki, A. T. 2001, PASJ, 53, 119
Osaki, Y. 1986, PASP, 98, 30
Owocki, S. P. 2005, in ASP Conf. Ser. nnn, IAU Symp. 215, Stellar Rotation, nnn
Perryman, M. A. C. 1997, Proc. of the ESA Symposium Hipparcos - Venice 97, ESA SP-402, 1
Porri, A., & Stalio, R. 1988, A&AS, 75, 371
Porter, J. M. 1999, A&A, 348, 512
Porter, J. M., & Rivinius, T. 2003, PASP, 115, 1153
Quirrenbach, A., Bjorkman, K. S., Bjorkman, J. E., et al. 1997, ApJ, 479, 477
Rivinius, Th., Baade, D., Štefl, S., et al. 1998, A&A, 333, 125
Rivinius, Th., Baade, D., Štefl, S., & Maintz, M. 2001, A&A, 379, 257
Rivinius, Th., Baade, D., & Štefl, S. 2003, A&A, 411, 229
Rohrmann, R. D. 2000, Ph.D. Thesis, Universidad Nacional de Córdoba, Argentina
Schaller, G., Schaerer, D., Meynet, G., et al. 1992, A&AS, 96, 269
Schmitz, F. 1983, A&A, 120, 234
Slettebak, A. 1982, ApJS, 50, 55
Stee, P., Bonneau, D., Lawson, P., et al. 1995, ed. E. Hog, & P. Kenneth Seidelmann, IAU Symp., 166, 149
Štefl, S., Baade, D., Rivinius, Th., et al. 2003a, A&A, 402, 253
Štefl, S., Baade, D., Rivinius, Th., et al. 2003b, A&A, 411, 167
Stoeckley, T. R. 1968, MNRAS, 140, 141
Struve, O. 1931, ApJ, 73, 94
Telting, J. H., & Schrijvers, C. 1997a, A&A, 121, 343
Telting, J. H., & Schrijvers, C. 1997b, A&A, 317, 723
Telting, J. H., & Schrijvers, C. 1997c, A&A, 343, 742
Thomas, R. N. 1965, Non-Equilibrium Thermodynamics in the Presence of a Radiation Field (Colorado: Univ. Colorado Press, Boulder)
Towsend, R. H. D., Owocki, S. P., & Howard, I. D. 2004, MNRAS, 350, 189
Tycner, Ch. 2004, Ph.D. Thesis, University of Toronto
Unno, W., Osaki, Y., Ando, H., & Shibahashi, H. 1989, Nonradial Oscillations of Stars, 2nd edn. (Univ. of Tokyo Press)
Vogt, S. S., & Penrod, G. 1983, ApJ, 275, 661
Wade, R. A., & Rucinski, S. M. 1985, A&AS, 60, 471
Waters, L. B. F. M. 1986, A&A, 162, 121
Waters, L. B. F. M., & Marlborough, J. M. 1994, ed. L. A. Balona, H. F. Henrichs, & J. M. Contel, IAU Symp., 162, 399
Wesselius, P. R., Duinene, R. J., van de jonge, A. R. W., et al. 1982, A&AS, 49, 427
Yudin, R. V. 2001, A&A, 368, 912
Zorec, J., & Briot, D. 1997, A&A, 318, 443
Zorec, J., Fremat, Y., & Leister, N. V. 2004, SF2A-2004: Semaine de l'Astrophysique Francaise, meeting held in Paris, France, June 14–18, 2004, ed. F. Combes, D. Barret, T. Contini, F. Meynadier, & L. Pagani (EdP-Sciences), Conf. Ser., 328
Zorec, J., Fremat, Y., & Cidale, L. 2005, A&A, 441, 235